Chiral Symmetry Breaking Phases at High Chemical Potential in the Nambu–Jona-Lasinio Model

Die chirale Symmetrie brechende Phasen bei hohen chemischen Potentialen im Nambu–Jona-Lasinio Modell

Bachelor-Thesis von Steven Vereeken

Tag der Einreichung:

1. Gutachten: PD Dr. Michael Buballa
2. Gutachten: Prof. Dr. Jochen Wambach

TECHNISCHE UNIVERSITÄT DARMSTADT

Department of Physics
Institute of nuclear physics
Nuclei, Hadrons and Quarks

Chiral Symmetry Breaking Phases at High Chemical Potential in the Nambu–Jona-Lasinio Model
Die chirale Symmetrie brechende Phasen bei hohen chemischen Potentialen im Nambu–Jona-Lasinio Modell

Vorgelegte Bachelor-Thesis von Steven Vereeken

1. Gutachten: PD Dr. Michael Buballa
2. Gutachten: Prof. Dr. Jochen Wambach

Tag der Einreichung:

Erklärung zur Bachelor-Thesis

Hiermit versichere ich, die vorliegende Bachelor-Thesis ohne Hilfe Dritter nur mit den angegebenen Quellen und Hilfsmitteln angefertigt zu haben. Alle Stellen, die aus Quellen entnommen wurden, sind als solche kenntlich gemacht. Diese Arbeit hat in gleicher oder ähnlicher Form noch keiner Prüfungsbehörde vorgelegen.

Darmstadt, den 27. April 2015

(Steven Vereeken)

Abstract

In this work we study chiral symmetry breaking phases at high chemical potential using the two-flavour Nambu–Jona-Lasinio model as an effective low-energy model of Quantum chromodynamics. First we discuss the theoretical framework and the case of a homogeneous mass modulation, while developing methods to calculate the phase transition boundaries. Afterwards, we choose an inhomogeneous mass modulation and transfer the methods to calculate the phase boundaries to the case of spatially dependent condensates. Since earlier works have found a second inhomogeneous phase ("continent") at high chemical potential, we mainly focus our research on that region of the phase diagram. Nonetheless, as it turns out, the continent does not only exist at high chemical potentials, but also at high temperatures regardless of the chemical potential, i.e. the continent encircles the restored phase entirely. Furthermore, the continent may extend to arbitrarily high temperatures and chemical potentials. Its existence is due to the medium contribution, which renders the vacuum contribution insignificant at high temperatures and chemical potential.

Zusammenfassung

In dieser Arbeit untersuchen wir die chirale Symmetrie brechende Phasen bei hohem chemischen Potential mittels dem zwei-Flavour Nambu–Jona-Lasinio Modell, einem effektiven Niederenergie-Modell der Quantenchromodynamik. Zunächst diskutieren wir das theoretische Gerüst und den Fall einer homogenen Massenmodulation, während wir auch Methoden entwickeln, um die Grenzen der Phasenübergänge zu berechnen. Danach wählen wir eine inhomogene Massenmodulation und übertragen die Methoden auf ortsabhängige Kondensate. Da frühere Arbeiten eine zweite inhomogene Phase ("Kontinent") bei hohen chemischen Potential entdeckt haben, werden wir uns hauptsächlich diesen Bereich des Phasendiagrammes zuwenden. Wie sich herausstellt, finden wir den Kontinent aber nicht nur bei genügend hohen chemischen Potentialen, sondern auch bei hohen Temperaturen, unabhängig vom chemischen Potential. Der Kontinent umschließt also die restaurierte Phase vollkommen. Des Weiteren kann der Kontinent auch bei beliebig hohen Temperaturen und chemischen Potentialen existieren. Der Grund seiner Existenz ist der Medium-Beitrag, welcher den Vakuum-Beitrag bei hohen Temperaturen und chemischen Potentialen bedeutungslos macht.

Contents

1 Introduction

The quest of understanding matter began in Ancient Greece, where philosophers coined the concepts of "atoms" (Greek for "indivisible") and "void" in order to describe it. Yet, it was not until the 19th century and the advancement in chemistry that atoms became widely accepted to be the constituents of matter. Further investigations led to the discovery of the first subatomic particle, the electron, by Thomson in 1897 [1], the postulation of the nucleus by Rutherford in 1911 [2] and the subsequent discovery of the proton, again by Rutherford, in 1917 [3]. In 1932 Chadwick discovered the neutron [4] and, in the same year, Heisenberg postulated that proton and neutron were two states of the same particle with different isospin [5]. During the next couple of decades, more and more particles were found. This led Gell-Mann and Zweig, independently of each other, to the postulation of quarks as the constituents of hadrons in 1964 [6, 7, 8]. Experiments conducted by Breidenbach et al. [9] and Bloom et al. [10] in 1968 comfirmed that the proton does indeed consist of smaller particles. This discovery eventually led to the formulation of quantum chromodynamics (QCD) in 1973 [11].
Today, QCD is widely accepted to properly describe the strong interaction between quarks. It features the phenomena of confinement, i.e. unbound quarks are not observed in nature, and asymptotic freedom, i.e. a vanishing coupling constant at high energy scales. Its Lagrangian is given by

$$\mathscr{L}_{QCD} = \overline{\psi}_{c_1,f}\left(i\not{\partial}_{c_1c_2} - m_f\delta_{c_1c_2}\right)\psi_{c_2,f} - \frac{1}{4}F^a_{\mu\nu}F^{a,\mu\nu}\,, \tag{1.1}$$

where $f \in \{u,d,s,c,b,t\}$ denote the flavours, $c_1, c_2 \in \{r,g,b\}$ the colours, m_f the mass of the flavour f, ψ and $\overline{\psi} = \psi^\dagger\gamma_0$ the quark fields, which are coupled to the gluon fields A^a_μ by the covariant derivative $D_\mu = \partial_\mu - igA^a_\mu\frac{\lambda^a}{2}$, λ^a being the Gell-Mann matrices and g the coupling constant, while $F^a_{\mu\nu} = \partial_\mu A^a_\nu - \partial_\nu A^a_\mu + gf^{abc}A^b_\mu A^c_\nu$ denotes the gluon field strength tensor, with f^{abc} being the structure constants of the corresponding Lie-algebra.
The QCD phase diagram has been subject of intense investigation. Lattice QCD, i.e. non-pertubative calculations, has produced several results for high temperatures and evidence for a crossover transition between the chirally broken and the chirally restored phase has been found [12]. However, lattice QCD exhibits a "sign-problem" [13] for non-vanishing chemical potentials. Therefore, one has to make use of other methods, for example effective models, like the Nambu–Jona-Lasinio model [14] or the Quark-Meson model, to study the region of non-vanishing chemical potential.
In this work we will make use of the Nambu–Jona-Lasinio model to investigate the phase diagram, which has been extensively done. It is widely believed, that quarks exhibit a homogeneously broken phase[1] in the low temperature, low chemical potential region and for higher temperatures, while in the region of low temperature and medium chemical potential, an inhomogeneous generated mass function becomes favoured, forming the "island". At higher energies, the generated mass function vanishes and the quark "enter" the chirally restored phase, which is believed to extend to arbitrarily high temperatures and chemical potentials. However, Buballa and Carignano [15] found a second inhomogeneously, chirally broken phase in the low temperature, high chemical potential region, "the continent", which seems to extend to arbitrarily high chemical potentials. Furthermore, it seems that the higher the chemical potential, the higher the temperature at which a second chirally broken phase exists.
In this work we will build on the results obtained in [15] and investigate the extend of the continent in the high chemical potential region. To that end, we will first derive an expression for the thermodynamic potential and choose a regularisation in chapter 2, before investigating the mass function and thermodynamic potential for spatially constant (homogeneous) mass modulations in chapter 3. In that chapter we will also develop methods with which we will calculate the phase transition boundaries and, hence, the phase diagram. In chapter 4, we will introduce a spatially dependent, i.e. inhomogeneous, mass modulation and transfer the methods to calculate the transition boundaries to that case. Furthermore we will discuss its phase diagram and, especially, the second inhomogeneous phase.

[1] The chiral symmetry is spontaneously broken and the quark's generated mass function is homogeneous

2 Nambu–Jona-Lasinio Model

In 1961 Nambu and Jona-Lasinio proposed a model explaining the dynamical mass generation for nucleons, in analogy with the theory of superconductivity [16, 17]. At that time quarks had yet to be discovered and the standard model, as well as the QCD, yet to be developed. Nevertheless the model successfully explained the dynamic mass generation of the constituents as the spontaneous breaking of chiral symmetry due to their interaction. Therefore it was later reinterpreted as an effective, low energy model of QCD by simply changing the nucleonic fields for quark fields. A downside of the model is the lack of gluon fields and their dynamics. This restricts the applicability severely as the basic QCD features of confinement and asymptotic freedom are not reflected. Nonetheless the Nambu–Jona-Lasinio (NJL) model reflects the chiral symmetry of QCD very well and is therefore used to study this phenomenon.

2.1 The NJL Lagrangian

In this work we will restrict ourselves to a $N_f = 2$ flavours version of the NJL model, including the up and down quark, a scalar-isoscalar and pseudoscalar-isovector four-point interaction. Yet, the model can be extended to include more flavours [18, 19] and more complicated interaction terms.
Our two-flavour NJL Lagrangian reads

$$\mathscr{L}_{NJL} = \overline{\psi}(i\partial\!\!\!/ - \underline{m})\psi + G_s((\overline{\psi}\psi)^2 + (\overline{\psi}i\gamma^5\vec{\tau}\psi)^2)\,. \tag{2.1}$$

ψ and $\overline{\psi} = \psi^\dagger\gamma^0$ describe quark and antiquark fields and are Dirac spinors in 3+1 dimensions with components in flavour and colour space (i.e. $4N_fN_c$ components in total). $\vec{\tau} = \left(\tau^1, \tau^2, \tau^3\right)^T$ denotes the Pauli matrices in isospin space, whereas G_s denotes the scalar coupling constant and has the dimension of an inverse mass squared. $\underline{m} = \mathrm{diag}(m_u, m_d)$ denotes the bare quark mass matrix, with m_u and m_d being the masses of the up and down quark, respectively, which we will assume to be degenerate, i.e. $m_u = m_d = m$.
The first term is the usual textbook Lagrangian for a free field obeying the Dirac equation. The second term reflects the four-point interaction and consists of a scalar ($\overline{\psi}\psi$) and pseudoscalar ($\overline{\psi}i\gamma^5\vec{\tau}\psi$) term. Due to the four-point interaction, the NJL model is non-renormalisable, which means that we will have to implement some sort of regularisation scheme later on (see section 2.3).

The NJL Lagrangian shares several important symmetries with QCD. Firstly, it is invariant under a global $U(1)_V$ phase transformation

$$\psi \to \exp(-i\alpha)\psi \quad \text{and} \quad \overline{\psi} \to \overline{\psi}\exp(i\alpha)\,, \tag{2.2}$$

with $\alpha \in \mathbb{R}$, leading to the conservation of the baryon number.
The assumption that the bare masses are degenerate renders the Lagrangian invariant under a vector $SU(2)_V$ transformation

$$\psi \to \exp\left(-i\vec{\tau}\cdot\vec{\theta}/2\right)\psi \quad \text{and} \quad \overline{\psi} \to \overline{\psi}\exp\left(i\vec{\tau}\cdot\vec{\theta}/2\right), \tag{2.3}$$

with $\vec{\theta} \in \mathbb{R}^3$, resulting in the conservation of isospin.
Performing an axial $SU(2)_A$ transformation

$$\psi \to \exp\left(-i\gamma^5\vec{\tau}\cdot\vec{\theta}/2\right)\psi \quad \text{and} \quad \overline{\psi} \to \overline{\psi}\exp\left(-i\gamma^5\vec{\tau}\cdot\vec{\theta}/2\right), \tag{2.4}$$

with $\vec{\theta} \in \mathbb{R}^3$, one can show that the Lagrangian is invariant if we assume the bare masses of the up and down quark to be degenerate.
The combination of the latter two $SU(2)_V \otimes SU(2)_A = SU(2)_L \otimes SU(2)_R$ is called chiral symmetry. It is explicitly broken by a non-vanishing bare mass as the Lagrangian is not invariant under $SU(2)_A$ transformations in that case. However, even in the chiral limit ($m \to 0$) the $SU(2)_A$ invariance is spontaneously broken by the condensates leading to the appearance of Goldstone bosons [20].

2.2 Thermodynamic Potential

In order to examine the spontaneous chiral symmetry breaking, we first have to derive an expression for the thermodynamic potential describing the system. In the following we use a slightly altered prescription that has been outlined in [21].
As we do not want to limit the number of particles within our system, our choice falls upon the grand potential ω per volume V

$$\frac{\omega(T,\mu)}{V} = \Omega(T,\mu) = -\frac{1}{\beta V}\log \mathscr{Z}(T,\mu)\,, \tag{2.5}$$

where T denotes the temperature, μ the chemical potential, $\beta = \frac{1}{T}$ the inverse temperature and $\mathscr{Z}$ the grand canonical partition function.
In statistical physics the partition function $\mathscr{Z}$ is given by

$$\mathscr{Z} = \mathbf{Tr}\, e^{-\beta(\hat{H}-\mu\hat{N})}\,,$$

where $\hat{H}$ denotes the Hamilton operator and $\hat{N}$ the particle number operator. This trace can be transformed into a functional integral of the form [22]

$$\mathscr{Z} = \int \mathscr{D}\overline{\psi}\,\mathscr{D}\psi\, \exp\left(-\int_{[0,\beta]\times V} d\,x_E\,(\mathscr{L}_E - \mu\mathscr{N})\right), \tag{2.6}$$

where we switched to Euclidean space with the Euclidean Lagrangian $\mathscr{L}_E = -\mathscr{L}_{NJL}(t=-i\tau)$ and the Euclidean position vector $x_E = (\tau,\vec{x})$ with the imaginary time $\tau = it$. Furthermore, we introduced the particle number density $\mathscr{N} = \overline{\psi}\gamma^0\psi$.
Before we are able to solve the functional integral and, therefore, obtain an expression for the grand potential, we linearise the Lagrangian using a mean-field approximation. To this end we expand the values of the scalar and pseudoscalar condensates around their respective expectation values. Using the abbreviations $\phi_S(\vec{x}) \doteq \left\langle\overline{\psi}\psi\right\rangle$ and $\vec{\phi}_P(\vec{x}) \doteq \left\langle\overline{\psi}i\gamma^5\vec{\tau}\psi\right\rangle$[1], while neglecting second order terms and assuming the condensates to be time independent, we obtain[2]

$$\begin{aligned}
\overline{\psi}\psi = \phi_S + \delta\phi_S \quad &\Leftrightarrow \quad \delta\phi_S = \overline{\psi}\psi - \phi_S \quad &\Rightarrow \quad \left(\overline{\psi}\psi\right)^2 \approx 2\,\overline{\psi}\phi_S\psi - \phi_S^2\,,\\
\overline{\psi}i\gamma^5\vec{\tau}\psi = \vec{\phi}_P + \delta\vec{\phi}_P \quad &\Leftrightarrow \quad \delta\vec{\phi}_P = \overline{\psi}i\gamma^5\vec{\tau}\psi - \vec{\phi}_P \quad &\Rightarrow \quad \left(\overline{\psi}i\gamma^5\vec{\tau}\psi\right)^2 \approx 2\overline{\psi}i\gamma^5\vec{\tau}\vec{\phi}_P\psi - \vec{\phi}_P^{\,2}\,.
\end{aligned} \tag{2.7}$$

After plugging this approximation into our Lagrangian and rearranging the terms, our mean-field Lagrangian in Euclidean space reads

$$\mathscr{L}_{MF} = \overline{\psi}\left(\gamma^0\partial_\tau - i\gamma^j\partial_j + m - 2G_S\left(\phi_S(\vec{x}) + i\gamma^5\vec{\tau}\cdot\vec{\phi}_P(\vec{x})\right)\right)\psi + G_S\left(\phi_S^2(\vec{x}) + \vec{\phi}_P^{\,2}(\vec{x})\right)\,. \tag{2.8}$$

Comparing this Lagrangian with the original one (eq. (2.1)), we can define a mass operator $\hat{M}(\vec{x})$, the so called constituent quark mass

$$\hat{M}(\vec{x}) = m - 2G_S\left(\phi_S(\vec{x}) + i\gamma^5\vec{\tau}\cdot\vec{\phi}_P(\vec{x})\right)\,. \tag{2.9}$$

Our mean-field Lagrangian now looks very much like the original. Especially if we switch back to Minkowski space

$$\mathscr{L}_{MF} = \overline{\psi}\left(i\partial\!\!\!/ - \hat{M}(\vec{x})\right)\psi - G_S\left(\phi_S^2(\vec{x}) + \vec{\phi}_P^{\,2}(\vec{x})\right)\,. \tag{2.10}$$

Identifying the inverse propagator

$$S^{-1} = \gamma^0\left[-\partial_\tau + \mu - \left(-i\gamma^0\gamma^j\partial_j + \gamma^0\hat{M}(\vec{x})\right)\right] = -\gamma^0\left(\partial_\tau - \mu + \mathscr{H}_{eff}(\vec{x})\right)\,, \tag{2.11}$$

[1] Strictly speaking we expand each component separatly, i.e. $\phi_P^a(\vec{x}) \doteq \left\langle\overline{\psi}i\gamma^5\tau^a\psi\right\rangle$ and combine them again aftewards.

[2] To provide better readability we omitted the space dependency of the condensates.

with the effective Hamiltonian $\mathscr{H}_{eff}$[3], and denoting the field-independent part as $\mathscr{V}(\vec{x}) \equiv G_S\left(\phi_S^2(\vec{x}) + \vec{\phi}_P^2(\vec{x})\right)$, the partition function reads

$$\mathscr{Z} = \int \mathscr{D}\overline{\psi}\,\mathscr{D}\psi\; exp\left(\int_{[0,\beta]\times V} dx_E\,(\overline{\psi}S^{-1}\psi - \mathscr{V}(\vec{x}))\right). \tag{2.12}$$

The field-independent part does not depend on any quark-spinor and, hence, it is nothing more than a constant factor regarding the functional integral. Therefore, we are able to split the partition function into two factors $\mathscr{Z}_{kin}$ (containing the functional integral) and $\mathscr{Z}_{cond}$.
The kinetic part of the partition function yields (see appendix B.1)

$$\mathscr{Z}_{kin} = \det\frac{S^{-1}}{T}.$$

As the partition function can be split into two factors, the grand potential splits up into two summands. In total we obtain

$$\Omega = \Omega_{kin} + \Omega_{cond} = -\frac{T}{V}\log\mathscr{Z}_{kin} - \frac{T}{V}\log\mathscr{Z}_{cond} = -\frac{T}{V}\log\det\frac{S^{-1}}{T} + \frac{T}{V}\int_{[0,\beta]\times V} d^4x_E\,\mathscr{V}(\vec{x}). \tag{2.13}$$

Using the relation $\log\det A = \mathbf{Tr}\log A$, we can rewrite the kinetic term of the grand potential (eq. (2.13)) as follows

$$\Omega_{kin} = -\frac{T}{V}\log\det\frac{S^{-1}}{T} = -\frac{T}{V}\mathbf{Tr}\log\frac{S^{-1}}{T}, \tag{2.14}$$

where the trace has to be taken over the Dirac, colour and flavour space, as well as over the Euclidean space $[0,\beta]\times V$. As the condensates $\phi_S(\vec{x})$ and $\vec{\phi}_P(\vec{x})$ only depend trivially on the colour, the trace over the colour space amounts to a degeneracy factor N_c.
Assuming that the pseudoscalar condensates have a fixed direction in isospin space, it follows that $\vec{\tau}\cdot\vec{\phi}_P(\vec{x}) = \tau^3\phi_P(\vec{x})$, if we choose the 3-direction. As a result the mass operator simplifies to

$$\hat{M}(\vec{x}) = m - 2G_S\left(\phi_S(\vec{x}) + i\gamma^5\tau^3\,\phi_P(\vec{x})\right)$$

and our effective Hamiltonian becomes a direct product of two Hamiltonians $\mathscr{H}_{eff} = \mathscr{H}_+ \otimes \mathscr{H}_-$, with

$$\mathscr{H}_+ = -i\gamma^0\gamma^j\partial_j + \gamma^0 M(\vec{x}) = \begin{pmatrix} i\sigma^j\partial_j & M(\vec{x}) \\ M^*(\vec{x}) & -i\sigma^j\partial_j \end{pmatrix}, \tag{2.15}$$

$$\mathscr{H}_- = -i\gamma^0\gamma^j\partial_j + \gamma^0 M^*(\vec{x}) = \begin{pmatrix} i\sigma^j\partial_j & M^*(\vec{x}) \\ M(\vec{x}) & -i\sigma^j\partial_j \end{pmatrix}, \tag{2.16}$$

where we used the chiral representation of the γ-matrices and the mass function

$$M(\vec{x}) = m - 2G_S\left(\phi_S(\vec{x}) + i\,\phi_P(\vec{x})\right) \tag{2.17}$$

As we assume isospin invariance, the two Hamiltonians are isospectral and we may restrict ourselves to one and, from now on, denote $\mathscr{H} \equiv \mathscr{H}_+$ by implication. The trace over flavour space now amounts to another degeneracy factor N_f.
We are now left with the trace over the Dirac and Euclidean space. For this, we assume that the inverse propagator in frequency-momentum space (cf. B.1)

$$S^{-1}_{p,p',n} = \left(i\gamma^0\omega_n + \gamma^0\mu - \gamma^j p_j\right)\delta_{\vec{p},\vec{p}'} - \sum_{\vec{q}} M_{\vec{q}}\,\delta_{\vec{p},\vec{p}'-\vec{q}} = \left(i\gamma^0\omega_n + \gamma^0\mu\right)\delta_{\vec{p},\vec{p}'} - \mathscr{H}_{\vec{p},\vec{p}'}$$

[3] This approach will be helpful later on as our task will be to diagonalise the effective Hamiltonian.

has already been diagonalised and call it $S_{p,n}$. We obtain

$$\begin{aligned} -\frac{1}{\beta V}\mathbf{Tr}_{V_4,Dirac}\log\left(\beta S^{-1}\right) &= -\frac{1}{\beta V}\mathbf{Tr}_{p,Dirac}\log\left(\beta S_{p,n}^{-1}\right) \\ &= -\frac{1}{\beta V}\log\left(\det\left(i\beta\gamma^0\right)\det\left(\omega_n - i\mu + i\mathscr{H}\right)\right) \\ &= -\frac{1}{\beta V}\sum_{E_\nu,n}\log\left(\beta^4\left(\omega_n - i\,\mu + iE_\nu\right)\right), \end{aligned} \tag{2.18}$$

where E_ν denote the eigenvalues of the Hamiltonian in frequency-momentum and Dirac space. We can calculate the sum over all n by summing Matsubara frequencies (cf. B.2) and obtain

$$\begin{aligned} \Omega_{kin} &= -\frac{N_c N_f}{\beta V}\sum_{E_\nu}\log\left[2\,\cosh\left(\beta\,\frac{E_\nu-\mu}{2}\right)\right] \\ &= -\frac{N_c N_f}{V}\sum_{E_\nu}\left(\frac{E_\nu-\mu}{2} + T\,\log\left(1+e^{-\frac{E_\nu-\mu}{T}}\right)\right). \end{aligned} \tag{2.19}$$

In general, the sum over E_ν depends on the chosen mass modulation and, hence, we cannot simplify it without the loss of generality. However, in the course of this work we will only consider mass modulations due to which the eigenvalues E_ν will come in pairs of opposite sign, i.e. $\pm|E_\nu|$. As a result, we can perform one part of the sum and our grand potential yields

$$\Omega_{kin} = -\frac{N_c N_f}{V}\sum_{E_\nu>0}\left(E_\nu + T\log\left(1+e^{-\frac{E_\nu-\mu}{T}}\right) + T\log\left(1+e^{-\frac{E_\nu+\mu}{T}}\right)\right), \tag{2.20}$$

where we now only have to sum over all positive eigenvalues.
Furthermore, we will be able to diagonalise the Hamiltonian analytically and, as a result, the respective Hamiltonians will be block diagonal in momentum-Dirac space. Therefore the sum over all $E_\nu > 0$ will become a sum over all momenta $\vec{p}$ and a sum over all positive eigenvalues $E_\lambda = E_\lambda(\vec{p}; M)$ of the respective Hamiltonian in Dirac space (cf. 3.1 and 4.2). As a result, our grand potential will take on the form

$$\begin{aligned} \Omega_{kin} &= -\frac{N_c N_f}{V}\sum_{\vec{p}}\sum_{E_\lambda>0}\left(E_\lambda + T\log\left(1+e^{-\frac{E_\lambda-\mu}{T}}\right) + T\log\left(1+e^{-\frac{E_\lambda+\mu}{T}}\right)\right) \\ &\to -N_c N_f\int\frac{d^3p}{(2\pi)^3}\sum_{E_\lambda>0}\left(E_\lambda + T\log\left(1+e^{-\frac{E_\lambda-\mu}{T}}\right) + T\log\left(1+e^{-\frac{E_\lambda+\mu}{T}}\right)\right). \end{aligned} \tag{2.21}$$

where E_λ denote the eigenvalues in Dirac space and we took the continuum limit.
The first term of the integrand describes the divergent zero-point energy of the vacuum $f_{vac}(E_\lambda)$, which we will have to regularise (see section 2.3). The second and third summands can be combined and describe the medium contribution $f_{med}(E_\lambda, T, \mu)$. They are also directly related to the quark and anti-quark occupation numbers, which is evident if one takes the derivative with respect to μ. Thus they describe the contributions of quark and antiquarks.

Now that we have calculated the kinetic part of the grand potential and have defined an effective mass M, our last task is to calculate the condensate contribution to the potential. For this purpose, we first solve the mass function (eq. (2.17)) for the sum of the scalar and pseudoscalar condensate and afterwards we take the square of the absolute value

$$\phi_S^2(\vec{x}) + \phi_P^2(\vec{x}) = \frac{|M(\vec{x})-m|^2}{4G_S^2}.$$

Plugging this into our condensate contribution $\mathscr{V}$, we obtain

$$\Omega_{cond} = \frac{T}{V}\int_{V_4} d^4x_E\,\frac{|M(\vec{x})-m|^2}{4G_S} = \frac{1}{4G_S V}\int_V d^3x\,|M(\vec{x})-m|^2\,, \tag{2.22}$$

where we performed the integration over the imaginary time, since we will consider the condensates to be time independent. However, we will allow a spatial modulation later on and, hence, we cannot perform the integration over position space just yet.
As a result, we have found an overall expression for our grand potential

$$\Omega = \frac{1}{V}\int_V d^3x\,\frac{|M(\vec{x})-m|^2}{4G_S} - \frac{N_c N_f}{V}\sum_{E_\nu>0}\left(f_{vac}(E_\nu)+f_{med}(E_\nu,T,\mu)\right), \tag{2.23}$$

with

$$f_{vac}(E_\nu) = E_\nu \qquad \text{and} \qquad f_{med}(E_\nu,T,\mu) = T\,\log\left(1+e^{-\frac{E_\nu+\mu}{T}}\right) + T\,\log\left(1+e^{-\frac{E_\nu-\mu}{T}}\right). \tag{2.24}$$

Apart from regularising the vacuum contribution f_{vac} and defining a modulation for our mass function, we are basically ready to evaluate the grand potential, and, thus, to examine the mass function, by looking for its global minimum with respect to $M(\vec{x})$. To that end we could minimise the potential directly. Or we could look for its extrema by searching for the roots of its functional derivative with respect to the constituent quark mass $M(\vec{x})$. Using the first procedure we would end up with all local minima while the latter would return all local maxima in addition to all local minima. Therefore we will have to calculate the values of the grand potential for all found solutions, regardless of the procedure we use, and by doing so we identify the global minimum of the potential. Repeating this procedure for several temperatures T with a fixed chemical potential μ or vice versa, will then give us the mass function in dependence of T or μ. In the course of this work we will employ the latter procedure for reasons which will become evident in section 3.3.

2.3 Regularisation

In the course of this work, we will only consider mass modulations due to which part of the sum over all eigenvalues E_ν in our kinetic grand potential (eq. (2.19)) will become a sum and subsequently, by taking the continuum limit, an integral over the momentum $\vec{p}$ and a sum over all positive Dirac eigenvalues E_λ (cf. ch. 3.1 and 4.2). That is, our kinetic potential will be of the form

$$\begin{aligned}\Omega_{kin} &= -\frac{N_c N_f}{V}\sum_{E_\nu}\left(\frac{E_\nu-\mu}{2}+T\,\log\left(1+e^{-\frac{E_\nu-\mu}{T}}\right)\right)\\ &\to -N_c N_f\int\frac{d^3p}{(2\pi)^3}\sum_{E_\lambda>0}\left(f_{vac}\left(E_\lambda(\vec{p};M)\right)+f_{med}\left(E_\lambda(\vec{p};M),T,\mu\right)\right)\\ &= -N_c N_f\left(\Omega_{vac}+\Omega_{med}\right),\end{aligned} \tag{2.25}$$

with f_{vac} and f_{med} as defined in eq. (2.24).
While the medium contribution Ω_{med} will be finite, the vacuum contribution Ω_{vac} will be infinite. And since the NJL-Lagrangian is non-renormalisable due to the four-point interaction, we have to make use of a regularisation scheme in order to render it finite.
All regularisation schemes have in common that they apply some sort of cutoff parameter Λ. Once one has chosen a regularisation scheme, the cutoff parameter can be determined in a way that the model reproduces known properties of the investigated particles, for example the constituent quark mass or the pion mass and pion decay constant in the vacuum. Yet not all schemes are suited for every problem, which basically means that we have to choose our regularisation scheme carefully, as not to get stuck with artifacts, which would limit our insight into the behaviour of said particles. In the following we briefly discuss two often applied regularization schemes. A more detailed discussion can be found in [23].

2.3.1 Sharp 3-Momentum Cutoff

Using a sharp three-momentum cutoff, we are able to render the vacuum potential Ω_{vac} finite by restricting the absolute value of the momentum to values lower than the cutoff ($p \leq \Lambda$)

$$\int\frac{d^3p}{(2\pi)^3}f_{vac}(\vec{p};M)\to\int^{\Lambda}\frac{d^3p}{(2\pi)^3}f_{vac}(\vec{p};M). \tag{2.26}$$

This regularization scheme has the advantage that the integral can be performed analytically in special cases. However, this scheme breaks Lorentz invariance and if we do not consider our mass modulation to be spatially constant the sharp 3-momentum cutoff would limit the coupled momenta. As we want to introduce a spatially dependent modulation later on, this regularisation scheme would therefore lead to unwanted artifacts and, hence, does not fulfill our requirements which is why we will not use it.

2.3.2 Pauli-Villars Regularisation

The Pauli-Villars regularisation renders the vacuum potential finite by subtracting a function with the same asymptotic behaviour as the original one, in our case f_{vac}

$$\int\frac{d^3p}{(2\pi)^3}f_{vac}(\vec{p};M)\to\int\frac{d^3p}{(2\pi)^3}\sum_{j=0}^{n}c_j\sqrt{f_{vac}^2(\vec{p};M)+j\,\Lambda^2}. \tag{2.27}$$

The cutoff parameter Λ acts on the quark energy in contrast to the sharp 3-momentum cutoff that acts on the quark momenta. Another difference is, that the Pauli-Villars regularisation is Lorentz invariant. The number of counterterms n depends on the degree of divergence of the original function. Although two counterterms would be sufficient in our case, as two will render the gap-equations (cf. chapter 3) finite, we will in fact use three in order to ensure better convergence and to render the thermodynamical potential finite as well. The coefficients c_j are

calculated in appendix C.2 and yield $c_j = \{1, -3, 3, -1\}$. As with a sharp 3-momentum cutoff, the integral can only be solved analytically in special cases. Therefore, we will have to calculate it numerically alongside the medium contribution. However, since this regularisation scheme renders the vacuum contribution finite without limiting the coupled momenta, we will use it and from this point onward the vacuum contribution f_{vac} is given by

$$f_{vac}(\vec{p}; M) = \sum_{j=0}^{n} c_j \sqrt{E_\lambda^2 + j\,\Lambda^2}\,.$$

3 Homogeneous Mass Modulation

After having developed the theoretical framework in the last chapter, we are now ready to actually define a mass modulation and to examine the mass function as well as the various phases exhibited by the quarks. In this chapter we will focus on a spatially constant condensate, i.e. $\phi_S(\vec{x}) = \phi_S$ and $\phi_P(\vec{x}) = \phi_P = 0$. As a result, we are dealing with a homogeneous mass function as $M(\vec{x}) = M$ holds.
We will start with calculating the grand potential and the corresponding gap equation. Afterwards we will discuss the numerical results.

3.1 Thermodynamic Potential

With a homogeneous mass modulation, the integral in the condensate part of the potential (eq. (2.22)) is performed trivially

$$\Omega_{cond} = \frac{1}{4G_S V}\int_V d^3x\,|M(\vec{x})-m|^2 = \frac{1}{4G_S V}\int_V d^3x\,(M-m)^2 = \frac{(M-m)^2}{4G_S}\,. \tag{3.1}$$

Concerning the kinetic part of the potential, our task is to find the eigenvalues of the Hamiltonian as eq. (2.19) shows. For that, we switch to momentum space using a Fourier transformation and find

$$\mathscr{H} = \begin{pmatrix} -\vec{\sigma}\cdot\vec{p} & M \\ M & \vec{\sigma}\cdot\vec{p}\end{pmatrix}. \tag{3.2}$$

Thus Hamiltonian is diagonal in momentum space, as well as block diagonal in momentum-Dirac space. Therefore, the sum over all general eigenvalues E_ν in eq. (2.20) splits into a sum over all momenta $\vec{p}$, which can be transformed into an integral by taking the continuum limit, and a sum over all positive eigenvalues E_λ of the Hamiltonian in Dirac space.
The Dirac space eigenvalues E_λ yield

$$E_\lambda = \pm\sqrt{\vec{p}^2+M^2}\,, \tag{3.3}$$

with a degeneracy factor of 2. Plugging those into eq. (2.21), our grand potential for a homogeneous mass modulation reads[1]

$$\Omega_{hom} = \frac{(M-m)^2}{4G_S} - \frac{N_c N_f}{\pi^2}\int_0^\infty dp\,p^2\left(\sqrt{\vec{p}^2+M^2} + T\,\log\left(1+e^{-\frac{\sqrt{\vec{p}^2+M^2}+\mu}{T}}\right) + T\,\log\left(1+e^{-\frac{\sqrt{\vec{p}^2+M^2}-\mu}{T}}\right)\right), \tag{3.4}$$

where we switched to spherical coordinates and performed the angular integration.

3.2 Spectral Density Function

In the previous section we derived an expression for the grand potential, in which a momentum integral is present. We can change that momentum integral into an energy integral by the means of substitution:

$$\int_0^\infty dp\,p^2\,(f_{vac}(p;M)+f_{med}(p,T,\mu;M)) = \int_0^\infty dE\,\rho(E,M)\,(f_{vac}(E)+f_{med}(E,T,\mu))\,.$$

The function $\rho(E,M)$ is called the spectral density function and "absorbs" the terms that are a result of the substitution. In our case (homogeneous constituent mass), the spectral function reads:

$$\rho(E;M) = \theta\left(E^2-M^2\right)E\sqrt{E^2-M^2}\,, \tag{3.5}$$

where $\theta(..)$ denotes the Heaviside step function and was introduced in order to perform the integral starting at zero.

[1] Our general expression for the grand potential restricts us to the positive energy eigenvalues E_λ.

3.3 Gap Equation

In this work we will evaluate the thermodynamic potential $\Omega(T,\mu;M)$ (eq. (3.4)) by calculating the roots of its derivative with respect to the constituent mass M, also called the gap equation,

$$\frac{\partial\Omega}{\partial M} \stackrel{!}{=} 0\,, \tag{3.6}$$

and compare the values of the grand potential at those solutions in order to identify the global minimum.
The calculation of the derivative is straightforward and yields

$$0 = M\left(1+\frac{2N_cN_fG_S}{\pi^2}\int_0^\infty dE\;\theta(E^2-M^2)\,\frac{E}{\sqrt{E^2-M^2}}\,(f_{vac}(E)+f_{med}(E,T,\mu))\right)-m\,, \tag{3.7}$$

where we rearranged factors as we are only interested in the zeros. We will use this equation to numerically find the value of the favoured constituent quark mass in dependence of the temperature T and chemical potential μ.
As our major interest lies in studying spontaneous symmetry breaking, we will mostly consider the so called chiral limit, i.e. a bare quark mass of $m = 0$. In this case the gap equation has the trivial solution $M = 0$. If the trivial solution is favoured for a fixed temperature and chemical potential, then chiral symmetry is restored.

3.4 Mass Function and Grand Potential

In this section we want to discuss the resulting mass function and grand potential. For that we firstly need to fix the parameters, i.e. the coupling constant G_S and the cutoff Λ. The parameters used are parameter set #1 listed in table C.1 of appendix C.1. They were obtained in the chiral limit, so if a bare quark mass is introduced they will not reproduce the exact same values of the observables. Nonetheless, in this chapter we will use a bare quark mass of $m = 5$ MeV simply for comparison, as the basic differences between the chiral limit and a finite bare quark mass will still be visible.

Figure 3.1 shows the mass function in dependence of the chemical potential at different temperatures with a finite bare mass quark (left) and in the chiral limit (right). In both, the mass function is discontinuous for low temperatures, which means that a first order phase transition occurs. At temperatures of around[2] $T = 75$ MeV and higher the mass function is continuous in the temperature and chemical potential. In the chiral limit, it exhibits a second order phase transition into the chirally restored phase, while with a finite bare quark mass a second order phase

[2] In the chiral limit, the critical point (CP), that is, the point at which the first order phase transition turns into a second order phase transition, is at $T \approx 74.12$ MeV and $\mu \approx 268.65$ MeV.

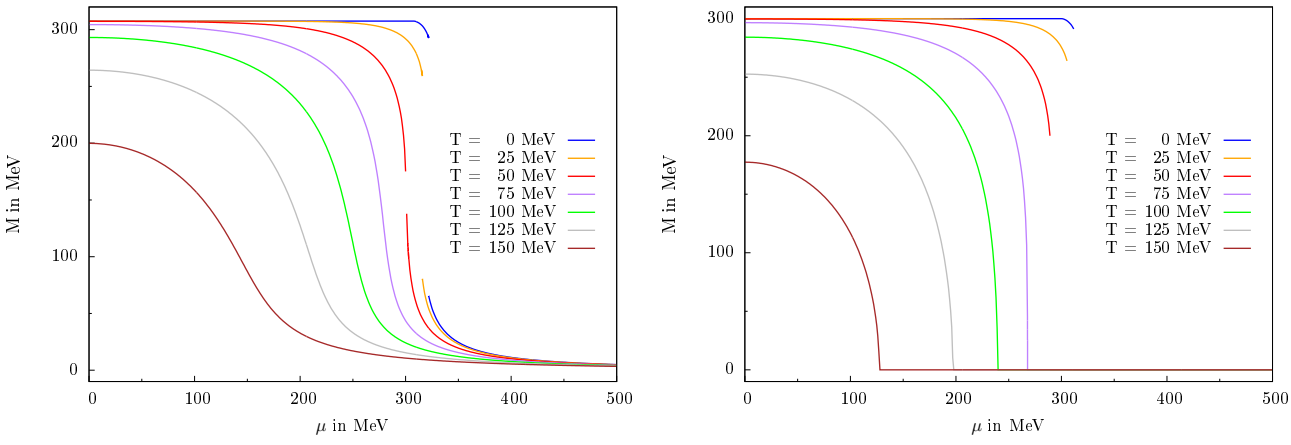

(a) $m = 5$ MeV **(b)** $m = 0$ MeV

Figure 3.1.: Mass function M in dependence of the chemical potential μ at different temperatures T for a bare quark mass of $m = 5$ MeV (left) and in the chiral limit (right) for a homogeneous mass modulation.

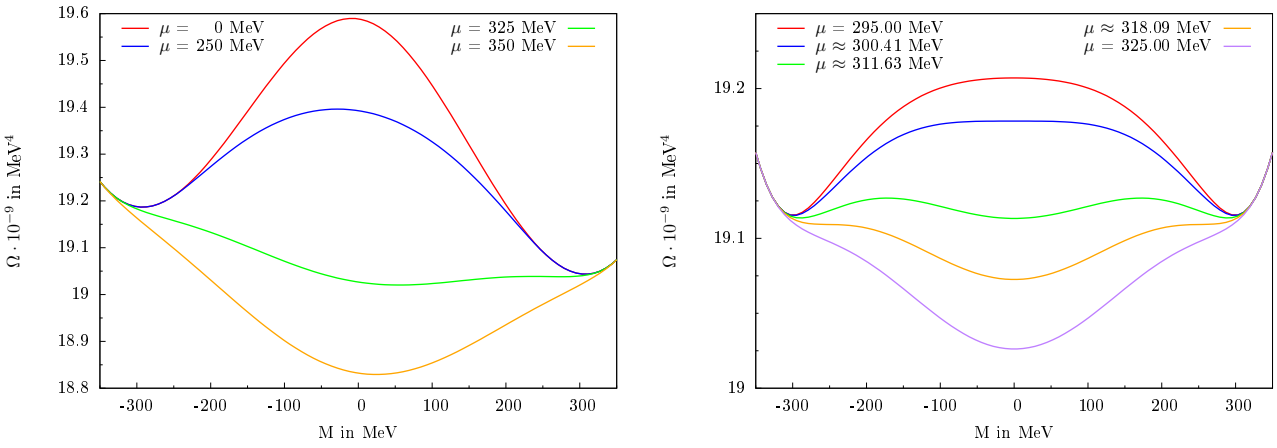

(a) $T = 0$ MeV, $m = 5$ MeV

(b) $T = 0$ MeV, $m = 0$ MeV

Figure 3.2.: Grand potential in dependence of the constituent mass for several chemical potentials in the zero temperature limit.

transition only occurs at the CP. For $m \neq 0$ we find a smooth crossover into a region where the chiral symmetry is restored approximately, if we move away from the CP. This illustrates very well the explicitly broken chiral symmetry we mentioned regarding the NJL Lagrangian (cf. section 2.1). We also note that the transitions in the chiral limit and with a finite bare quark mass occur at approximately the same chemical potential.

Figure 3.2 shows the grand potential in dependence of the constituent mass M for various chemical potentials at a temperature of $T = 0$. With a finite bare quark mass, we can once again plainly see the explicitly broken chiral symmetry, as we cannot exchange M and $-M$. Yet, it shows the same behavior as the right figure, where we operate in the chiral limit: The closer to the first order phase transition, the lower the potential around/at $M = 0$ until (in the chiral limit at about $\mu \approx 311.63$ MeV) both minima are at equal height, from which point onward the minima at $M = 0$ are preferred and chiral symmetry is restored (approximately in case of a finite bare quark mass). The figure on the right illustrates another behavior that occurs around first order phase transitions: the appearance of a spinodal region. At a chemical potential of $\mu \approx 300.41$ MeV the maximum at $M = 0$ turns into a minimum of the potential and therefore into a possible, yet energetically metastable, state. After the phase transition the previously favoured state with a generated mass becomes metastable until a chemical potential of $\mu \approx 318.09$ MeV, where it disappears and only one possible state is left. This spinodal region is unique to first order phase transitions.

Next, we briefly want to discuss the behavior of the grand potential in the chiral limit around a second order phase transition for completeness. This is presented in figure 3.3 at a temperature of $T = 100$ MeV. One can see that the potential behaves differently in comparison with a first order transition: the maximum at $M = 0$ does not turn into a minimum before the phase transition. Moreover, the favored constituent mass "moves" continuously toward that maximum until they coincide. If we were to add a finite bare quark mass, the behavior of the minima would not change. The maximum at around $M = 0$ would, on the other hand, move to the left until the merger with the left, i.e. negative, minimum takes place. At that point (yellow line; 3rd from below) the curvature vanishes and the phase transition occurs.

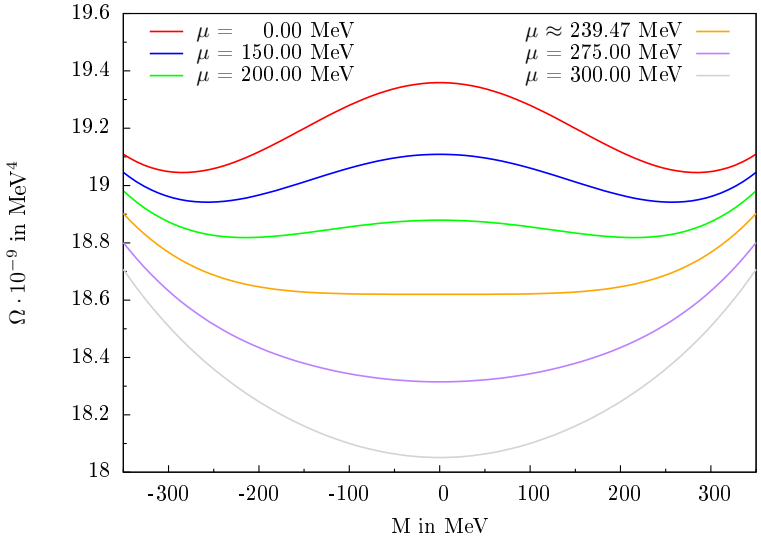

Figure 3.3.: Grand potential in dependence of the constituent mass M for several chemical potentials at a temperature of $T = 100$ MeV and in the chiral limit.

3.5 Phase Diagram

In this section we would like to calculate and discuss the phase diagram. Since only the phase boundaries enter into the phase diagram, we do not have to calculate the self-consistent solution of eq. (3.7) for every point (T, μ). Instead, using the chiral limit, we can calculate the lines at which the phase transition takes place by solving a system of equations. Since we will use the chiral limit when we introduce an inhomogeneous mass modulation in the next chapter, we will use it in this chapter as well. If one is not using the chiral limit, phase transition boundaries can be obtained by calculating various susceptibilities, which would be beyond the scope of this work. In the following, we will first derive equation(s) for the various lines that might be present in a phase diagram. Afterward, we will calculate and discuss the phase diagram itself.

To that end we divide eq. (3.7) by M. This does not change the non-trivial solutions, i.e. $M \neq 0$, but we get rid of the trivial one. The gap equation then reads

$$0 = 1 + \frac{2N_c N_f G_S}{\pi^2} \int_0^\infty dE\ \theta(E^2 - M^2) \frac{E}{\sqrt{E^2 - M^2}} \left(f_{vac}(E) + f_{med}(E, T, \mu)\right) . \tag{3.8}$$

Now, we can take the limit $M \to 0$ without automatically solving the equation. Yet, the resulting equation is the same as taking the second derivative of the grand potential (eq. (3.4)) with respect to M at $M = 0$ and setting it to zero

$$0 = 1 + \frac{2N_c N_f G_S}{\pi^2} \int_0^\infty dE\ \left(f_{vac}(E) + f_{med}(E, T, \mu)\right) . \tag{3.9}$$

By solving this equation for T (μ) we are able to calculate the temperature (chemical potential) at which, for a given chemical potential (temperature), the maximum of the grand potential at $M = 0$ actually turns into a minimum or in other words the point (T, μ) at which the grand potential has a saddle point at $M = 0$. Above the CP this behavior corresponds to a second order phase transition (cf. section 3.4). For temperatures lower than the temperature at the critical point the mass function exhibits a different behavior. The result we obtain for that region corresponds to the left boundary of the spinodal region, that is, the region within which the grand potential has two local minima.
The right boundary of said region can be calculated as well. For that we need a second equation, as the constituent mass will not be zero. Since that boundary will also show us the last points (T, μ) at which a non-trivial solution to the gap equation exists, we may use the derivative of eq. (3.8) with respect to M

$$0 = \frac{2N_c N_f G_S}{\pi^2} \int_0^\infty dE\ \theta(E^2 - M^2) \frac{EM}{(E^2 - M^2)^{3/2}} \left(f_{vac}(E) + f_{med}(E, T, \mu)\right) . \tag{3.10}$$

This function will give us the mass M at which a saddle point occurs in the grand potential for a given T and μ or if the mass M is known. Solving both equations (eq. (3.9) and eq. (3.10)) simultaneously for M and T (or μ), while the chemical potential (temperature) is fixed, will give us the right boundary and the constituent mass M at the boundary.
Using the same method, yet a different second equation, we are able to calculate the point (T, μ) at which both minima of the grand potential within the spinodal region are at equal height, i.e. both solutions of the gap equation yield the same result when plugged into the grand potential. We know that one solution is at $M = 0$ while for the other $M \neq 0$ holds. Therefore we can use the free energy as second equation

$$\begin{aligned} 0 &= \Omega_{hom}(T,\mu;M) - \Omega_{hom}(T,\mu;M=0) \\ &= \frac{M^2}{4G_S} - \frac{N_c N_f}{\pi^2}\int_0^\infty dE\, E\left(\theta\left(E^2-M^2\right)\sqrt{E^2-M^2}-E\right)\left(f_{vac}(E)+f_{med}(E,T,\mu)\right). \end{aligned} \tag{3.11}$$

The temperature (chemical potential) and mass M that solve both equations are the respective parameters at which the mass function exhibits a first order phase transition (cf. section 3.4).

Figure 3.4 shows the phase diagram we obtain using the methods described above. Clearly visible is, that the spinodal boundary lines only occur around a first order phase transition and they, as well as the first order transition boundary, end in the CP, from which point onward the phase transition is of second order. To the right of the transition boundaries the chiral symmetry is restored while to the left we find a chirally broken phase with a non-vanishing generated mass.

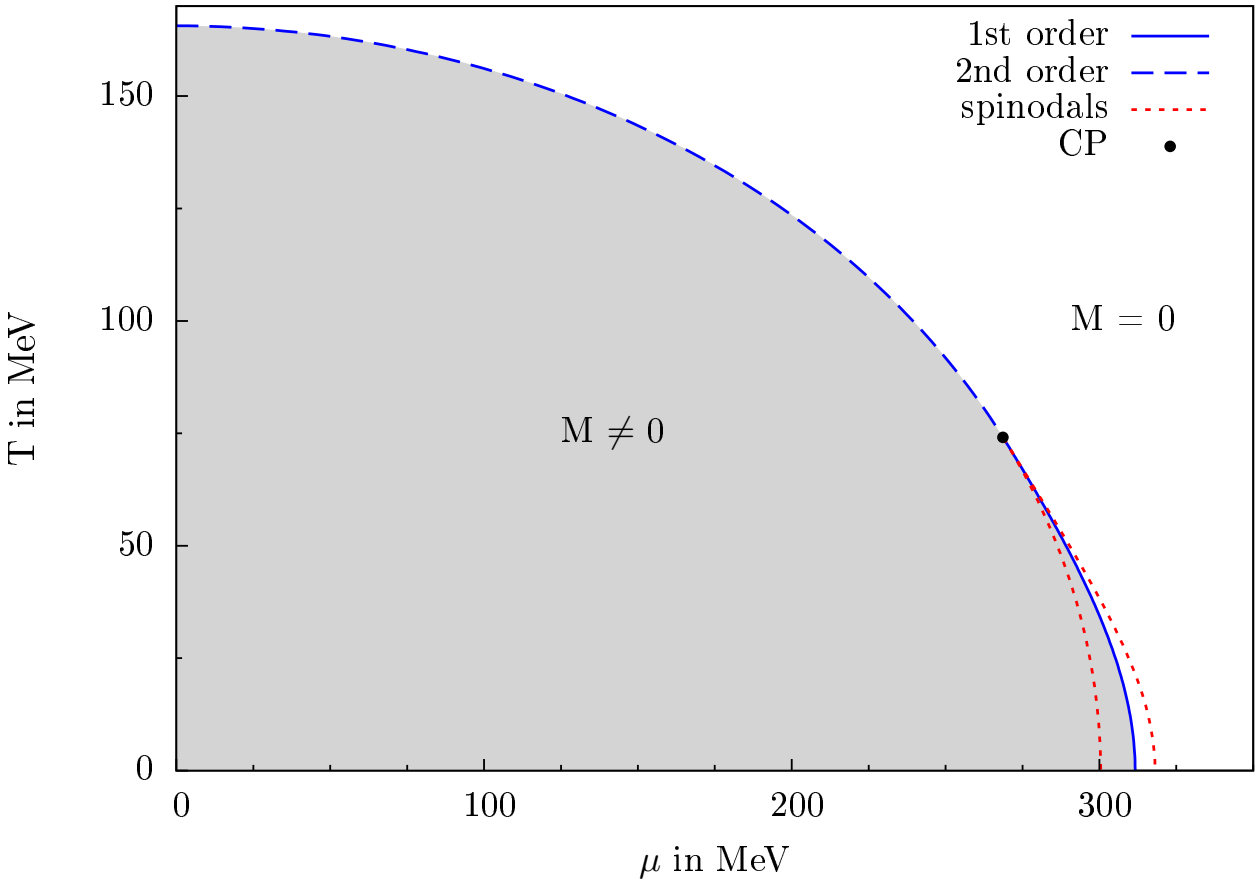

Figure 3.4.: Phase diagram of the NJL model with a homogeneous effective mass modulation in the chiral limit. The shaded area denotes the chirally broken phase. With a finite bare quark mass there would be no second order phase transition, but a smooth crossover.

4 Inhomogeneous Mass Modulation

After having examined the case of a homogeneous mass modulation in the last chapter, we will now turn our focus to spatially dependent modulations. However, we will only consider periodic modulations, i.e. there exist linear independent vectors $\vec{a}_j$ with $j \in \{1,2,3\}$ so that $M\left(\vec{x}+\vec{a}_j\right) = M(\vec{x})$ holds. We will also stay in the chiral limit throughout this chapter. We further simplify the problem by limiting the inhomogeneous mass modulation to one dimension. Without loss of generality, we choose the z-direction, i.e. $\vec{x} = (0,0,z)^T$.

4.1 Ansatz for a Mass Modulation

The simplest ansatz for an inhomogeneous mass modulation is a single plane wave, the so called chiral density wave (CDW)

$$M(\vec{x}) = \Delta\, e^{i\vec{q}\cdot\vec{x}}\,, \tag{4.1}$$

where Δ denotes the amplitude and $\vec{q} = (0,0,q)$ the wave vector.
Writing out the exponential function and comparing it with eq. (2.17), we can see that this modulation corresponds to a sinusoidal behaviour of the scalar and pseudoscalar condensates with

$$\phi_S(\vec{x}) = -\frac{\Delta}{2G_S}\cos(\vec{q}\cdot\vec{x}) \quad \text{and} \quad \phi_P(\vec{x}) = -\frac{\Delta}{2G_S}\sin(\vec{q}\cdot\vec{x})\,. \tag{4.2}$$

Alternatively we could use a real ansatz for our modulation that has a lower free energy like for example a one dimensional solitonic modulation with [24]

$$M(z) = \Delta\,\nu\frac{sn(\Delta z|\nu)cn(\Delta z|\nu)}{dn(\Delta z|\nu)}\,,$$

where sn, cn and dn are Jacobi elliptic functions, while Δ and ν denote the variational parameters or a sinusoidal one with

$$M(\vec{x}) = \Delta\cos(\vec{q}\cdot\vec{x})\,,$$

where Δ and $\vec{q}$ have the same meaning as for the CDW. In contrast to the CDW and the solitonic modulation, no analytic expression for the dispersion relation of the real sinusoidal ansatz is known, which means that we would have to implement some sort of numerical diagonalization procedure for the Hamiltonian. However, assuming we would do that, neither the solitonic nor the sinusoidal nor the CDW modulation exhibit different phases, although the order of the transitions and the size of those phases may differ, which means that we would not get a better insight into the mechanisms of spontaneous chiral symmetry breaking, but solely a better insight into the ground state. Therefore the simplest ansatz for a mass modulation suffices and we will use the CDW in this work.

4.2 Thermodynamic Potential

In section 2.2 we calculated an expression for the grand potential (eq. (2.23)) within which the eigenvalues of the Hamiltonian in the kinetic term still have to be found and the integration over position space in the condensate term still has to be performed. In this chapter we will do both, where finding the eigenvalues E_ν of the Hamiltonian will be the major task. Hence, we will start by following [25] to compute those eigenvalues and afterwards we will perform the integration over position space in the condensate part.
There are a few ways to calculate the eigenvalues of the Hamiltonian. For example, as outlined in [26] we could diagonalise the Hamiltonian in momentum space and use a procedure given in [27] in the similar context of crystalline color superconductivity. If no analytical expression for the energy eigenvalues can be found, this method can be used. It is described in detail in, for example, [21] or [28]. However we will take a different approach. Plugging our mass modulation into our Hamiltonian (eq. (2.15)) we find

$$H(\vec{x}) = -i\gamma^0\gamma^j\partial_j + \gamma^0\Delta\left(\cos(\vec{q}\vec{x}) + i\gamma^5\sin(\vec{q}\vec{x})\right) = -i\gamma^0\gamma^j\partial_j + \gamma^0\Delta e^{i\gamma^5\vec{q}\cdot\vec{x}}\,. \tag{4.3}$$

Obtaining the eigenvalues means solving the eigenvalue problem $H\psi = E\psi$. To that end we now perform a local rotation of the quark fields using

$$\psi = e^{-\frac{i}{2}\gamma^5\vec{q}\cdot\vec{x}}\psi' = U(\vec{x})\psi'\,,$$

which transforms our eigenvalue equation into $H'\psi' = E\psi'$, with

$$\begin{aligned}
H' &= U^\dagger(\vec{x})\,H\,U(\vec{x}) \\
&= e^{\frac{i}{2}\gamma^5\vec{q}\cdot\vec{x}}\left[-i\gamma^0\gamma^j\partial_j + \gamma^0\Delta e^{i\gamma^5\vec{q}\vec{x}}\right]e^{-\frac{i}{2}\gamma^5\vec{q}\cdot\vec{x}} \\
&= -e^{\frac{i}{2}\gamma^5\vec{q}\cdot\vec{x}}i\gamma^0\gamma^j\partial_j e^{-\frac{i}{2}\gamma^5\vec{q}\cdot\vec{x}} + e^{\frac{i}{2}\gamma^5\vec{q}\cdot\vec{x}}\gamma^0\Delta e^{i\gamma^5\vec{q}\vec{x}}e^{-\frac{i}{2}\gamma^5\vec{q}\cdot\vec{x}} \\
&= -e^{\frac{i}{2}\gamma^5\vec{q}\cdot\vec{x}}i\gamma^0\gamma^j\left(\partial_j e^{-\frac{i}{2}\gamma^5\vec{q}\cdot\vec{x}} + e^{-\frac{i}{2}\gamma^5\vec{q}\cdot\vec{x}}\partial_j\right) + e^{\frac{i}{2}\gamma^5\vec{q}\cdot\vec{x}}\gamma^0\Delta e^{\frac{i}{2}\gamma^5\vec{q}\cdot\vec{x}} \\
&= -e^{\frac{i}{2}\gamma^5\vec{q}\cdot\vec{x}}i\gamma^0\gamma^j\left(-e^{-\frac{i}{2}\gamma^5\vec{q}\cdot\vec{x}}\frac{i}{2}\gamma^5 q_j + e^{-\frac{i}{2}\gamma^5\vec{q}\cdot\vec{x}}\partial_j\right) + e^{\frac{i}{2}\gamma^5\vec{q}\cdot\vec{x}}\gamma^0\Delta e^{\frac{i}{2}\gamma^5\vec{q}\cdot\vec{x}} \\
&= -e^{\frac{i}{2}\gamma^5\vec{q}\cdot\vec{x}}e^{-\frac{i}{2}\gamma^5\vec{q}\cdot\vec{x}}i\gamma^0\gamma^j\left(-\frac{i}{2}\gamma^5 q_j + \partial_j\right) + e^{\frac{i}{2}\gamma^5\vec{q}\cdot\vec{x}}e^{-\frac{i}{2}\gamma^5\vec{q}\cdot\vec{x}}\gamma^0\Delta \\
&= -i\gamma^0\gamma^j\left(-\frac{i}{2}\gamma^5 q_j + \partial_j\right) + \gamma^0\Delta \\
&= -i\gamma^0\gamma^j\partial_j + \gamma^0\gamma^j\gamma^5 Q_j + \gamma^0\Delta\,,
\end{aligned} \tag{4.4}$$

where we used that $\{\gamma^5,\gamma^j\} = 0 = \{\gamma^5,\gamma^0\}$, while we abbreviated $Q_j = \frac{q_j}{2}$.
As the Hamiltonian does not depend on $\vec{x}$ any longer, we are able to use a standard plane-wave ansatz and set $\psi' = e^{i\vec{p}\vec{x}}\psi''$ to obtain

$$\begin{aligned}
H'\psi' = \left(-i\gamma^0\gamma^j\partial_j + \gamma^0\gamma^j\gamma^5 Q_j + \gamma^0\Delta\right)e^{i\vec{p}\vec{x}}\psi'' = e^{i\vec{p}\vec{x}}\left(\gamma^0\gamma^j p_j + \gamma^0\gamma^j\gamma^5 Q_j + \gamma^0\Delta\right)\psi'' = e^{i\vec{p}\vec{x}}\,E\,\psi'' \\
\iff \qquad \left(\gamma^0\gamma^j p_j + \gamma^0\gamma^j\gamma^5 Q_j + \gamma^0\Delta\right)\psi'' = E\,\psi''\,.
\end{aligned} \tag{4.5}$$

As with the homogeneous mass modulation (cf. ch. 3.1), the sum over all general eigenvalues E_ν (cf. eq. (2.20)) splits into a sum over all momenta $\vec{p}$, which we will again turn into an integral over all energies E by using the spectral density function, and a sum over all positive eigenvalues E_λ of the Hamiltonian in Dirac space. For the latter, we obtain

$$E_\pm^2 = \vec{p}^{\,2} + \vec{Q}^2 + \Delta^2 \pm 2\sqrt{\Delta^2\vec{Q}^2 + \left(\vec{p}\cdot\vec{Q}\right)^2}\,. \tag{4.6}$$

Our next step is using these eigenvalues to calculate the spectral density function ρ_{CDW} and plug it into our grand potential. The spectral density function has been calculated by Nickel [24] and yields

$$\begin{aligned}
\rho_{CDW}(E,Q;\Delta) = \frac{E}{2}\Big(\theta(E-Q-\Delta)\sqrt{(E-Q)^2-\Delta^2} + \theta(E-Q+\Delta)\,\theta(E+Q-\Delta)\sqrt{(E+Q)^2-\Delta^2} + \\
+\theta(Q-E-\Delta)\left(\sqrt{(E+Q)^2-\Delta^2} - \sqrt{(E-Q)^2-\Delta^2}\right)\Big)\,,
\end{aligned} \tag{4.7}$$

where we restricted ourselves to $Q, \Delta, E > 0$ for simplicity.
We are now left with calculating the condensate part of the potential. Plugging our CDW mass modulation into eq. (2.22) yields

$$\Omega_{cond} = \frac{1}{V}\int_V d^3x \, \frac{\left|\Delta e^{i\vec{q}\cdot\vec{x}}\right|^2}{4\,G_S} = \frac{\Delta^2}{4G_S V}\int_V d^3x = \frac{\Delta^2}{4G_S}\,. \tag{4.8}$$

As a result our overall grand potential Ω is given by

$$\Omega = \frac{\Delta^2}{4G_S} - \frac{N_f N_c}{\pi^2}\int_0^\infty dE\,\rho_{CDW}(E,Q;\Delta)\,\left(f_{vac}(E) + f_{med}(E,T,\mu)\right)\,. \tag{4.9}$$

In case of $Q = 0$ we obtain, of course, the homogeneous grand potential.

4.3 Gap Equation

Having calculated the grand potential in the previous section, we are now ready to calculate the gap equations. In contrast to the homogeneous case, where we only had to vary one parameter, in the inhomogeneous case we have to vary two: Δ and Q. This means that we have need of two gap equations, resulting from the stationary conditions

$$\frac{\partial\Omega}{\partial\Delta} \overset{!}{=} 0 \quad \text{and} \quad \frac{\partial\Omega}{\partial Q} \overset{!}{=} 0\,, \tag{4.10}$$

which have to be fulfilled simultaneously in order to obtain the local minima of the grand potential. As with a homogeneous mass modulation, the points (Δ, Q) of the global minima of the grand potential are obtained by comparing the values for the grand potential at all found solutions.
The calculation of the respective derivatives is straightforward and, after some rearrangements, yield[1]

$$G_\Delta = 2\,G_S\,\frac{\partial\Omega}{\partial\Delta} = \Delta\left(1 + \frac{G_S N_f N_c}{\pi^2}\int_0^\infty dE\,\rho_\Delta\,\left(f_{vac}(E) + f_{med}(E,T,\mu)\right)\right) = 0\,, \tag{4.11}$$

$$G_Q = \frac{2\,\pi^2}{N_c\,N_f}\,\frac{\partial\Omega}{\partial Q} = \int_0^\infty dE\,\rho_Q\,\left(f_{vac}(E) + f_{med}(E,T,\mu)\right) = 0\,, \tag{4.12}$$

where we abriged

$$\rho_\Delta = E\left(\frac{\theta(E+Q-\Delta)\theta(E-Q+\Delta) + \theta(Q-\Delta-E)}{\sqrt{(E+Q)^2-\Delta^2}} + \frac{\theta(E-Q-\Delta) - \theta(Q-\Delta-E)}{\sqrt{(E-Q)^2-\Delta^2}}\right)\,, \tag{4.13}$$

$$\rho_Q = E\left((E+Q)\,\frac{\theta(E+Q-\Delta)\theta(E-Q+\Delta) + \theta(Q-\Delta-E)}{\sqrt{(E+Q)^2-\Delta^2}} - |E-Q|\,\frac{\theta(E-Q-\Delta) + \theta(Q-\Delta-E)}{\sqrt{(E-Q)^2-\Delta^2}}\right)\,. \tag{4.14}$$

Note that we obtain the homogeneous gap equation (eq. (3.7)) for $Q = 0$.

[1] The derivatives of the Heaviside functions either do not contribute or cancel each other out.

4.4 Calculating the Phase Boundaries

In order to find equations that will give us the phase transition boundaries of a CDW mass modulation, we can transfer the methods developed in section 3.5 to our current needs, since the general mechanisms at the phase boundaries should not change. Yet, there are several differences we have to account for, the major one being that we are now dealing with a second parameter which results in at least one additional equation needed to calculate the respective boundaries.
Once again, we start with getting rid of the trivial solution of G_Δ (eq. (4.11)) by dividing it by Δ

$$1 + \frac{G_S N_f N_c}{\pi^2} \int_0^\infty dE\, \rho_\Delta \, (f_{vac}(E) + f_{med}(E,T,\mu)) = 0\,. \tag{4.15}$$

The limit $\Delta \to 0$ does exist and yields

$$1 + \frac{G_S N_f N_c}{\pi^2} \int_0^\infty dE\, E \left(\frac{1}{E+Q} + \frac{1}{E-Q} \right) (f_{vac}(E) + f_{med}(E,T,\mu)) = 0\,. \tag{4.16}$$

This means that we can once again use it as our first equation to obtain the second order phase transition boundary. It is intuitive to consider the gap equation of Q as second equation. However, at $\Delta = 0$ the gap equation of Q equals zero for all Q, which makes it useless in its current form. As a workaround we can expand G_Q around $\Delta = 0$:

$$G_Q(\Delta) = \frac{1}{2} \frac{\partial^2 G_Q}{\partial \Delta^2}\bigg|_{\Delta=0} \Delta^2 + \frac{1}{24} \frac{\partial^4 G_Q}{\partial \Delta^4}\bigg|_{\Delta=0} \Delta^4 + \mathcal{O}(\Delta^6) = 0\,. \tag{4.17}$$

Dividing this equation by Δ^2 will rid us of the trivial solution $\Delta = 0$ without changing the non-trivial solutions and we can once again take the limit $\Delta \to 0$. Omitting irrelevant constant factors, we obtain [2]

$$\int_0^\infty dE\, E \left(\frac{1}{(E-Q)^2} - \frac{1}{(E+Q)^2} \right) (f_{vac}(E) + f_{med}(E,T,\mu)) = 0\,. \tag{4.18}$$

However, if implemented in full, this equation turns out to be too challenging numerically. Yet, comparing it with eq. (4.16), we see that eq. (4.18) is the derivative of eq. (4.16) with respect to Q. Therefore, we are able to numerically calculate the derivative of eq. (4.16) with respect to Q using the difference quotient, which is less demanding numerically, and use it as our second equation. As a result, we can simultaneously solve equations (4.16) and (4.18) at a given temperature (chemical potential) in order to obtain the chemical potential (temperature) at which a second order phase transition takes place while also getting the value of Q at those boundaries.
Since Q might be zero, we will, of course, find all "homogeneous" boundary lines corresponding to eq. (4.15) at $Q = 0$ (cf. section 3.5) as well. Thus, for temperatures below the critical point we will again obtain solutions with $Q = 0$ that give us the left boundary of the homogeneous spinodal region. As we are dealing with an inhomogeneous mass modulation there might also exist an inhomogeneous spinodal region with at least one solution where $Q \neq 0$. Unfortunately we are currently unable to calculate the boundaries of said region. However, in analogy to the homogeneous spinodal region, the inhomogeneous spinodal region should encapsulate a first order phase transition from or to the inhomogeneous phase.
In section 3.3 we only needed two equations to calculate the first order transition boundary. Now we will need four, as it might not be a first order transition to the restored phase with $\Delta = 0$ and $Q = 0$, but it may be a first order phase transition from the homogeneously broken phase with $\Delta \neq 0$ and $Q = 0$ to the inhomogeneously broken phase with $\Delta \neq 0$ and $Q \neq 0$, or vice versa. Therefore, we cannot set the "second" Δ to zero and use the free energy. Yet, at both minima the grand potential will still yield the same value at the first order phase transition, i.e.

$$\Omega(T,\mu,Q,\Delta_1) - \Omega(T,\mu,0,\Delta_2) = 0\,. \tag{4.19}$$

As second equation we can simply use eq. (4.12), while eq. (4.11) or eq. (4.15) gives us the third equation. As fourth equation we can use the homogeneous gap equation which corresponds to eq. (4.11) at $Q = 0$. Solving those four equations simultaneously for Q, Δ_1, Δ_2 and μ or T will give us the first order transition boundary from the homogeneous to the inhomogeneous phase, or vice versa if that should exist.

[2] Once again, the derivatives of the Heaviside functions either do not contribute or cancel each other out.

4.5 Numerical Results

In this chapter we present the numerical results obtained using the methods developed above. We will push the validity of the NJL model to its limit and investigate the phases at high chemical potential and high temperature.

Figure 4.1 shows the phase diagram for a vacuum constituent quark mass of $M = 300$ MeV that we obtained using the methods described in the previous section. We can see that for temperatures below the Lifshitz point [3] (LP) and low chemical potential a first order phase transition from the homogeneously to the inhomogeneously broken phase occurs, while above the LP the transition is to the restored phase and of second order, complying with the results of section 3.4. The inhomogeneous first order phase transition takes place only slightly before what would be a homogeneous first order transition to the restored phase. The result is an inhomogeneous "island" that, compared with the homogeneous case, extends the overall broken phase toward higher chemical potentials. Eventually this island gives way to the restored phase by a second order phase transition. At even higher chemical potential a second inhomogeneous phase ("continent") arises for which the transition is of second order. This phase extends to high chemical potential (cf. figure 4.2) as well as high temperature (cf. figure 4.3) and encloses the restored phase entirely, making it some sort of "lake".

[3] Commonly used to describe the point at which three phase transition boundaries meet. In our case it coincides with the critical point of chapter 3.

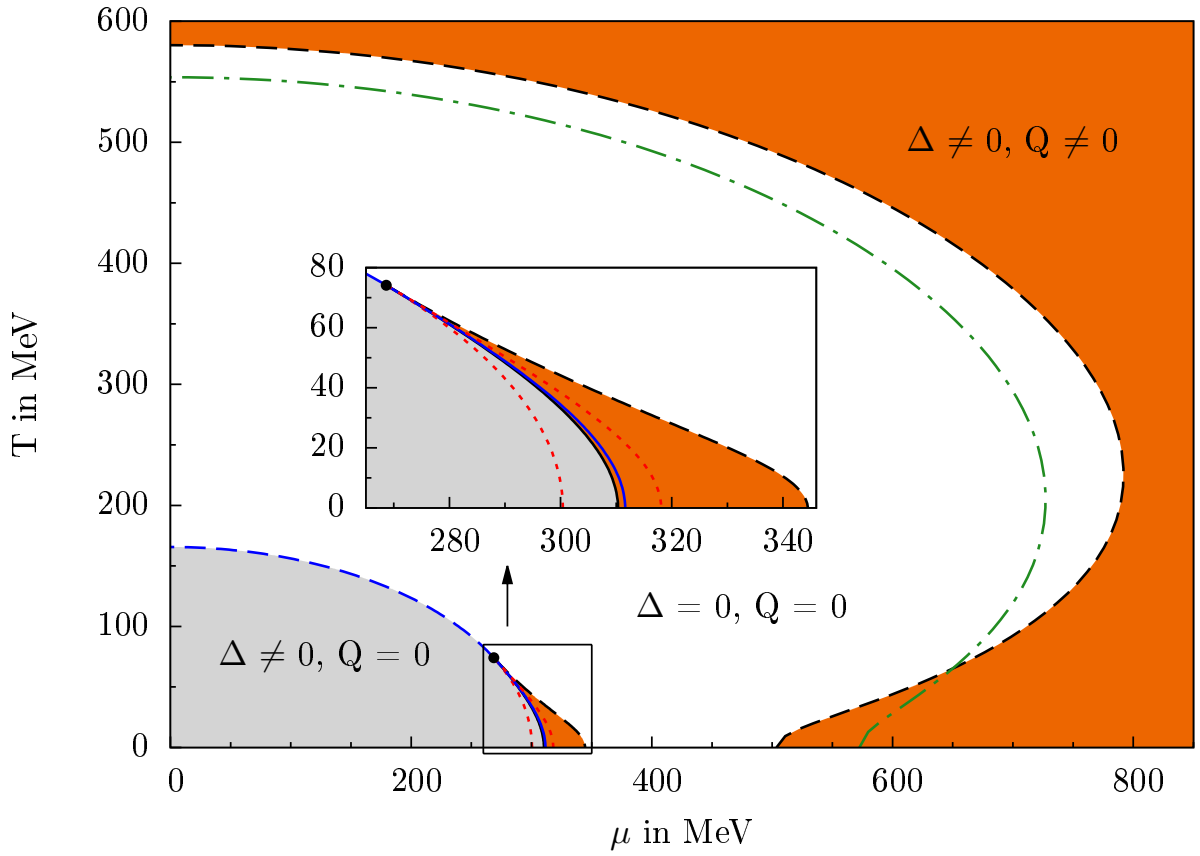

Figure 4.1.: Phase diagram for a vacuum constituent quark mass of $M = 300$ MeV. The grey shaded area denotes the homogeneously broken phase, while the orange area denotes the inhomogeneously broken phase. A white background illustrates the restored phase. The black dot symbolises the LP. Dashed lines represent second order phase transitions, solid lines correspond to first order transitions. Blue lines correspond to the homogeneous, black lines to inhomogeneous phase transitions. The red dotted lines show two (homogeneous) spinodal boundaries. The dashed dotted green line denotes the continent boundary in the no-sea approximation.

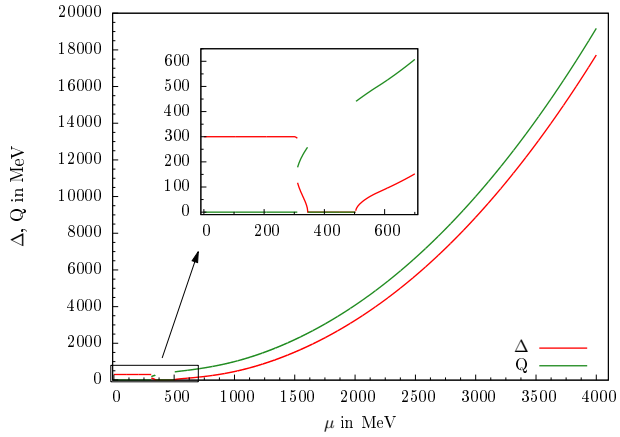

(a) $T = 0$ MeV

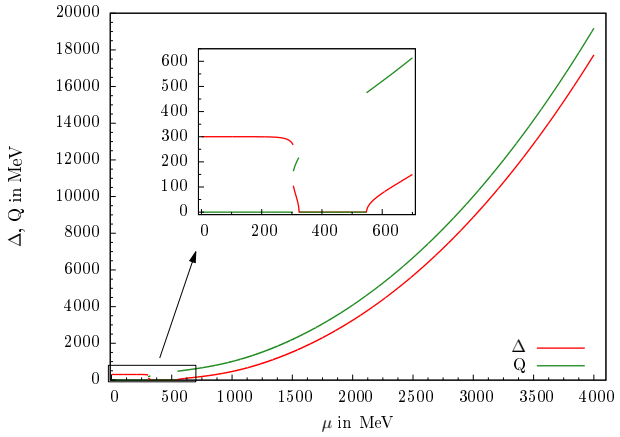

(b) $T = 25$ MeV

Figure 4.2.: Parameter Δ and Q in dependence of the chemical potential μ at a temperature of $T = 0$ (left) and $T = 25$ MeV (right). It is clearly visible that both parameters strictly increase in value for arbitrarily high chemical potential.

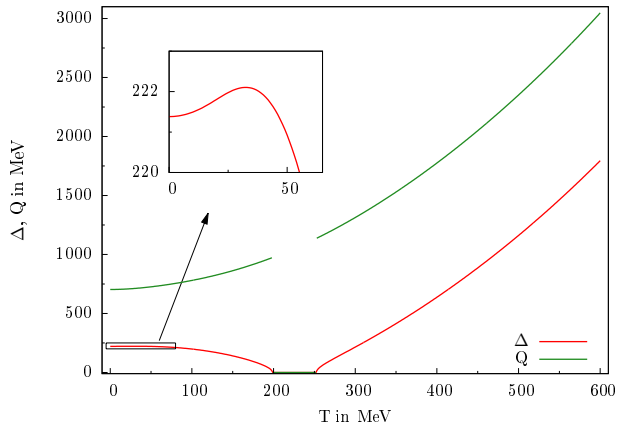

(a) $\mu = 790$ MeV

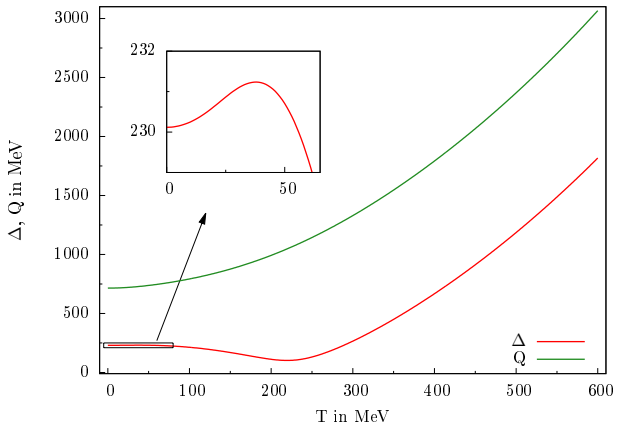

(b) $\mu = 800$ MeV

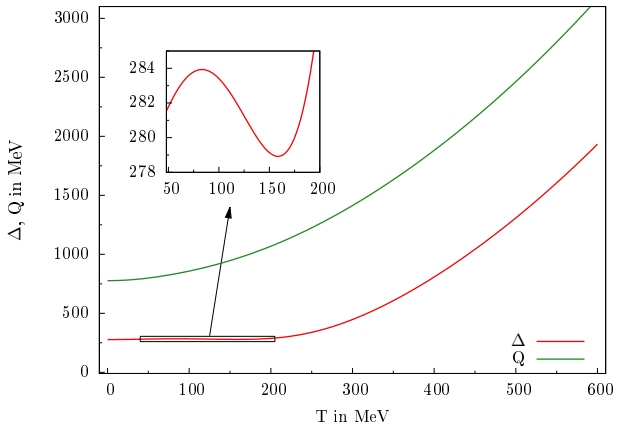

(c) $\mu = 850$ MeV

Figure 4.3.: Parameter Δ and Q in dependence of the temperature T at a chemical potential of $\mu = 790$ (upper left), $\mu = 800$ MeV (upper right) and $\mu = 850$ (below). Obviously, at a fixed but high chemical potential, the amplitude Δ does not steadily decrease immediately at low, yet growing temperatures, but increases initially, forming a local maximum. At higher or lower chemical potential this is not case.

In figure 4.2 we present the favoured values of the amplitude Δ and wave number Q in dependence of the chemical potential μ at temperatures of $T = 0$ and $T = 25$ MeV. One can see that the island is characterised by the appearance of a non-zero wave number and by a discontinuity in the amplitude Δ. The latter drops to zero at the transition to the restored phase, while the wave number strictly increases. At the continent boundary the amplitude is continuous and strictly increases henceforth. The wave number on the other hand has a discontinuity once again. In fact it seems as if an inhomogeneous solution "hides" itself at $\Delta = 0$, where the grand potential is degenerate, and steadily "moves" to higher values of the wave number, reappearing at a certain temperature and chemical potential.

Figure 4.3 shows the amplitude Δ and wave number Q in dependence of the temperature T at certain chemical potentials μ. Basically we see that the same characteristics apply as for the case of a fixed temperature and varied chemical potential. The difference being that we now only capture the continent and, hence, no first order phase transition or homogeneously broken phase occurs. Curiously enough, the amplitude first increases before decreasing and, at a chemical potential of $\mu = 790$ MeV, inducing a second order phase transition to the restored phase. At higher temperatures another second order phase transition takes place. The amplitude now shows exactly the same characteristics as for a fixed temperature and high chemical potential. At higher chemical potential no phase transition and therefore, no restored phase occurs. Nonetheless, the behaviour of the amplitude at lower temperatures does not change immediately as can be seen for the chemical potentials of $\mu = 800$ MeV and $\mu = 850$ MeV. However, this changes at higher chemical potentials, where the amplitude strictly increases and therefore behaves similar to the case of a fixed temperature and varied chemical potential.

All these characteristics also appear when fixing the parameters to obtain a higher or lower constituent mass in the vacuum (cf. figure 4.4), which is basically obtained by a higher or lower coupling constant, respectively. Additionally, a higher coupling constant moves the continent towards lower chemical potential and temperature until it merges with the island. A lower coupling constant on the other hand, moves the continent towards higher chemical potential and temperature. However, a lower coupling constant also moves the homogeneously broken phase, this time towards lower chemical potential and temperature, while a higher coupling constant moves that phase towards higher chemical potential and temperature. A higher coupling constant also widens the island, while a lower one narrows it.

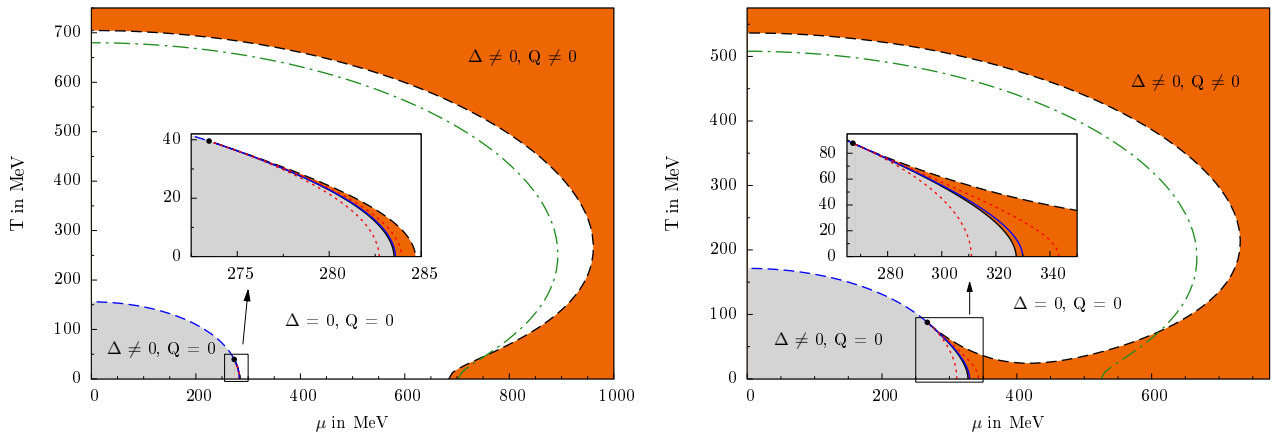

(a) $M = 250$ MeV **(b)** $M = 330$ MeV

Figure 4.4.: Phasediagram for a constituent quark mass of $M = 250$ MeV (left) and $M = 330$ MeV (right) for comparison. The illustrations are the same as in figure 4.1. The parameter sets (cf. tab. C.1) are #2 (left, $M = 250$ MeV) and #3 (right, $M = 330$ MeV).

4.6 Examining the Continent

Before further investigating the appearance of the continent we first would like to briefly recap the mechanisms leading to the formation of the continent at low temperatures as reported in [15]. To that end, we subtract the free energy of the restored phase from the general grand potential

$$\Omega - \Omega_{rest} = \frac{\Delta^2}{4G_S} - \frac{N_f N_c}{\pi^2} \int_0^\infty dE \, [\rho_{CDW}(E,Q;\Delta) - \rho_{CDW}(E,0,0)] \, [f_{vac}(E) + f_{med}(E,T,\mu)] \, . \tag{4.20}$$

If the difference is smaller than 0, then the chiral symmetry is broken, otherwise it is restored. Since the condensate term is positive at all times, i.e. it disfavours chiral symmetry breaking, the integral must be positive in order to allow for preferred inhomogeneous phases. Figure 4.5 shows the functions that enter the integral. The regularised vacuum contribution f_{vac} is negative for all energies (red solid line in fig. 4.5a) and its minimum is at $E = 0$. The medium contribution f_{med}, on the other hand, is positive for all energies, its maximum being at $E = 0$. As a result, the sum $f = f_{vac} + f_{med}$ becomes less negative with increasing T and μ at small energies until changing its sign. In other words, with increasing T and μ, the vacuum contribution will eventually lose out to the medium contribution at small energies, while always winning at higher energies. This is also illustrated in figure 4.5a for the values $(T,\mu) = (0, 600)$ MeV (green dashed line) and $(T,\mu) = (600, 0)$ MeV (blue dotted line).
Thus, the spectral density function of the self-consistent solutions $\rho_{CDW}(E,Q;\Delta)$ minus its restored counterpart $\rho_{CDW}(E,0;0)$ should, in principle, exhibit similar characteristics regarding the sign change. As figure 4.5b shows, similar mechanisms do indeed apply. For $Q = 0$ the difference $\delta\rho$ of both densities of states is negative for all energies (red solid line in fig. 4.5b) and its absolute value increases with increasing Δ. Therefore, in the vacuum, the integrand of equation (4.20) is positive for all $\Delta \neq 0$ and the free energy gain is stabilised by the condensate term at some optimum value of Δ. For increasing temperature and chemical potential, however, a non-trivial solution will become more and more disfavoured, as the integrand becomes less and less positive until eventually changing sign. This explains the non-existence of the continent in case of a homogeneous mass modulation. Keeping $\Delta \neq 0$ fixed and increasing Q, $\delta\rho$ becomes less and less negative at small energies until changing its sign in that region for $Q \gtrsim \Delta$, while it remains negative for $E \gtrsim Q - \frac{\Delta^2}{4Q}$ at all times (cf. green dotted and blue dashed line in fig. 4.5b). Hence, an inhomogeneous phase can only exist if $Q > \Delta$ holds. Note that, at a given T and μ, we can always find a tuple (Δ, Q) for which the integrand is positive for all energies. Yet said tuple does not need to correspond to a minimum of the potential. In fact, this is approximately true only for the case of low temperatures and high (but not arbitrarily high) chemical potentials. Considering this case, we can estimate the value of Q within the continent for small T (cf. fig. 4.1). In this region the sum f

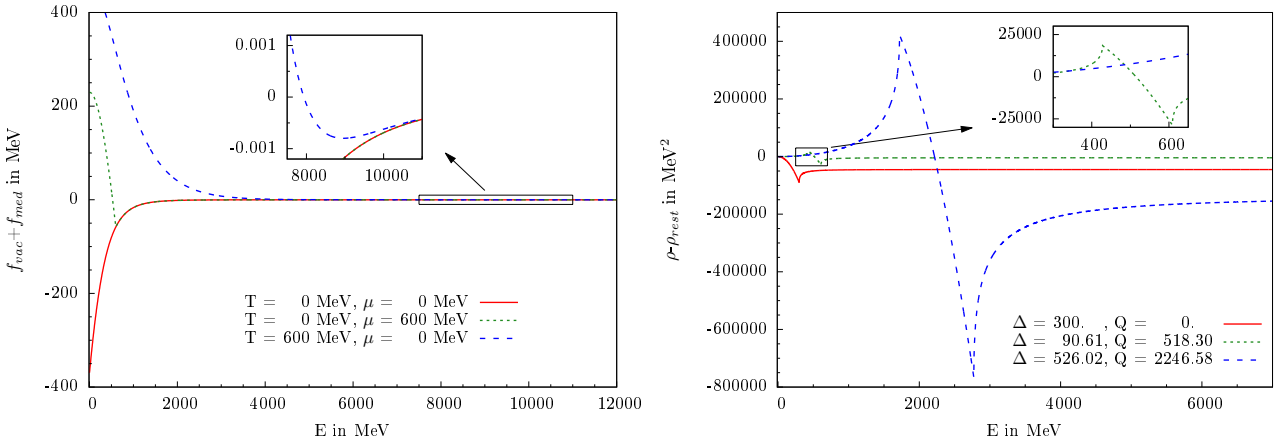

(a) $f_{vac} + f_{med}$.

(b) $\rho - \rho_{rest}$. Δ and Q are given in MeV

Figure 4.5.: Both factors of the integrand of the free energy $\Omega - \Omega_{rest}$ in dependence of the energy E. All graphs were calculated using the stable values for Δ and Q at the specified temperatures T and chemical potentials μ. For $T = 0$ and $\mu = 0$ those are $\Delta = 300$ MeV and $Q = 0$. At $T = 0$ and $\mu = 600$ MeV we find $\Delta \approx 90.61$ MeV and $Q \approx 518.30$ MeV, while at $T = 600$ MeV and $\mu = 0$ the stable solutions are $\Delta \approx 526.02$ MeV and $Q \approx 2246.58$ MeV.

changes sign at $E \approx \mu$, allowing us to roughly estimate the wave number with $Q \approx \mu$. For high temperatures we are unable to find such an approximation. While $\delta\rho$ does not depend on the temperature or the chemical potential, and, hence, keeps its overall shape, the sum f becomes larger than zero for almost all energies and the negative part of f can be neglected (cf. dashed blue line in fig. 4.5a). A favoured inhomogeneous solution now exists, if the positive part of $\delta\rho$ is amplified in a way that it becomes larger than the negative part of $\delta\rho$, while the latter has to be "cut" by the sum f. This is basically achieved by an optimum value for Q, while Δ mainly widens the peaks. Nonetheless, the optimum value of Q also depends on Δ. As in the homogeneous case, the value of Δ is stabilised by the condensate term. As an overall result we can conclude that the appearance of inhomogeneous phases is induced by the medium contribution f_{med}, which complies with the results of [29, 30, 31].

In order to further investigate the appearance of the continent, we now apply the "no-sea" approximation, i.e. we set our cutoff to $\Lambda = 0$. This basically amounts to equating the vacuum contribution f_{vac} to zero in the grand potential (eq. (4.9)) and the gap equations (eq. (4.11) and eq. (4.12)). As we do not fit the values of the coupling constants G_s to this "regularisation", but keep using the coupling constants given in table C.1, the results we obtain will not reflect real existing phases. Nonetheless, as we have seen above, inhomogeneous phases are induced by the medium and at high temperatures and high chemical potentials the medium contribution overcomes the vacuum contribution. From those arguments it follows that the continent should also exist with this "regularisation". And indeed, using the "no-sea" approximation we find that only the continent exists (the beginning is given by the green dashed dotted line in fig. 4.1 and 4.4), the onset being a second order phase transition. As one can see, for low temperatures the vacuum contribution with the PV regularisation "pulls" the continent towards the vacuum, while it "pushes" the continent away from the vacuum at higher temperatures. This can be attributed to the favoured value of the wave number Q: At low temperatures the preferred wave number is relatively small, keeping the positive part of $\delta\rho$ at small energies E (cf. fig. 4.5b), i.e. a region, where the vacuum contribution f_{vac} has the most impact on the sum f.

Taking a closer look at the spectral density function reveals, that

$$\lim_{\Delta\to\infty} \rho_{CDW}(E, Q; \Delta) = 0 \qquad \text{and} \qquad \lim_{Q\to\infty} \rho_{CDW}(E, Q; \Delta) = E^2 \tag{4.21}$$

for all finite Q, T, μ and Δ, T, μ, respectively. Since the condensate part of the potential Ω is positive for all Δ and there are no singularities within ρ, it follows that the potential is bounded from below for all Δ and fixed Q, T, μ. This does not necessarily have to hold for all Q and fixed Δ, T, μ. However, $\rho_{CDW}(E, 0, 0) = E^2$ and, therefore,

$$\lim_{Q\to\infty} (\Omega - \Omega_{rest}) = \frac{\Delta^2}{4G_S} \geq 0 \tag{4.22}$$

holds for all finite Δ, T, μ. As we expect that the value of Q becomes very large for extremely high temperatures and chemical potentials (cf. fig. 4.2 and 4.3) this result seems to indicate that the continent does not extend to arbitrarily high temperatures and chemical potentials. On the other hand, from the figures 4.2 and 4.3 we may also conclude that, if the continent does extend to arbitrarily high temperatures and chemical potentials, the self-consistent solutions for Δ and Q would be approximately equal, i.e. $\frac{\Delta}{Q} \approx 1$. Using this approximation, the spectral density function becomes negative for all $E \gtrsim \frac{3Q}{4}$. If we now take the limit $Q \to \infty$, the integrand will be positive for all E. Thus, the continent may very well extend to arbitrarily high temperatures and chemical potentials.

5 Conclusion

In this work we have studied chiral symmetry breaking at high chemical potential and temperature for a spatially dependent, periodic mass modulation in the two-flavour Nambu–Jona-Lasinio model.
We started with the introduction of the NJL-Lagrangian and the derivation of the general thermodynamic potential in chapter 2. At the end of that chapter we briefly discussed two often used regularisation schemes and chose the Pauli-Villars regularisation. We proceeded with introducing the easier case of homogeneous condensates and discussed the numerical results, including the phase diagram, in chapter 3. Furthermore, we developed methods to calculate the phase boundaries and other lines that might appear in a phase diagram in section 3.3. Afterwards we turned our focus towards spatially dependent mass modulations in chapter 4. After having chosen our mass modulation to be the chiral density wave (sec. 4.1), we calculated the corresponding thermodynamic potential (sec. 4.2). In section 4.3 we computed the equations needed to examine the inhomogeneous mass function and transferred the methods to calculate the phase transition boundaries to the case of inhomogeneous condensates. The latter were then used to calculate the phase diagram. We found that the second inhomogeneous phase does not only seem to extend toward (probably arbitrarily) high chemical potential, but toward high temperatures as well. We further examined the mass function in dependence of the chemical potential and temperature, respectively, and found both to behave more or less the same. At a fixed but high chemical potential, i.e. at the beginning of the continent at low temperatures, the amplitude of the mass modulation Δ and the wave number Q in dependence of the temperature first increase, before decreasing and allowing a second order phase transition to the restored phase. At higher temperatures another second order phase transition to the chirally broken phase takes place once again. This behaviour still occurs in a region where the continent is not "interrupted" by a restored phase, yet, it disappears completely for even higher chemical potentials. We went on to discuss the mechanism leading to the appearance of the continent and, using the no-sea approximation, we saw that the continent still shows. However, the actual shape of the continent boundary in the $T - \mu$ plane does depend on the vacuum contribution and, consequently, on the regularisation.
Afterward we discussed the spectral density function explicitly. We found that the potential is bounded from below for all amplitudes Δ and fixed wave numbers Q and vice versa. However, we cannot rigorously prove that this holds if we vary both variables at the same time, although we do believe this to be the case. Lastly, we found that the continent may very well extend to arbitrarily high temperatures and chemical potentials.

A Conventions

In this work we will use natural units (unless explicitly stated otherwise), i.e.

$$\hbar = c = k_B = 1\,.$$

We will use greek letters to indicate Lorentz indices running from 0 to 3, while Latin letters as indices run from 1 to 3. Furthermore, we use the Einstein convention at all times, i.e.

$$a_j b^j = \sum_j a_j b^j\,.$$

When calculating in Minkowski space we use the metric $g_{\mu\nu} = \mathrm{diag}\{1,-1,-1,-1\}$.
In the chiral representation the γ-matrices read:

$$\gamma^0 = \begin{pmatrix} 0 & \mathbb{1} \\ \mathbb{1} & 0 \end{pmatrix},\ \gamma^j = \begin{pmatrix} 0 & \sigma^j \\ -\sigma^j & 0 \end{pmatrix},\ \gamma^5 = \begin{pmatrix} -\mathbb{1} & 0 \\ 0 & \mathbb{1} \end{pmatrix},$$

where $\mathbb{1}$ denotes the 2×2 identity matrix and σ^j the Pauli matrices:

$$\sigma^1 = \begin{pmatrix} 0 & 1 \\ 1 & 0 \end{pmatrix},\ \sigma^2 = \begin{pmatrix} 0 & -i \\ i & 0 \end{pmatrix},\ \sigma^3 = \begin{pmatrix} 1 & 0 \\ 0 & -1 \end{pmatrix}.$$

A.1 Fourier Decomposition

In this work we will transform spinors according to

$$\begin{aligned} \psi(\vec{x}) &= \frac{1}{\sqrt{V}} \sum_{\vec{p},n} e^{-i(\omega_n \tau - \vec{p}\vec{x})}\, \psi_n(\vec{p})\,, \\ \overline{\psi}(\vec{x}) &= \frac{1}{\sqrt{V}} \sum_{\vec{p},n} e^{i(\omega_n \tau - \vec{p}\vec{x})}\, \overline{\psi}_n(\vec{p})\,, \end{aligned} \tag{A.1}$$

where $\omega_n = \frac{(2n+1)\pi}{\beta}$ denote the fermionic Matsubara frequencies, with the inverse temperature $\beta = \frac{1}{T}$.
In the course of this work, we will only consider inhomogeneous mass modulations that are periodic and time independent. That is, there exist linear independent vectors $\vec{a}_j$, $j \in \{1,2,3\}$, so that $M\left(\vec{x}+\vec{a}_j\right) = M\left(\vec{x}\right)$ and wave vectors $\vec{q}_k$ which obey $\vec{q}_k \cdot \vec{a}_j = 2\pi \cdot n_{jk}\,,\ n_{jk} \in \mathbb{Z}\ \forall j,k$. Therefore, we will Fourier transform the mass according to

$$M(\vec{x}) = \sum_{\{\vec{q}\}} e^{i\vec{q}\vec{x}} M_{\vec{q}}\,. \tag{A.2}$$

.

B Calculations for the General Grand Potential

B.1 Calculating the Functional Integral

In section 2.2 we have to calculate the functional integral in order to obtain an expression for the partition function. To solve it we start with eq. (2.12) and first concentrate on the exponent, the Euclidean action S_E, while neglecting the condensate contribution as it does not affect the outcome. Using a discrete Fourier transformation on the spinors (cf. eq. (A.1)) and the mass function (cf. eq. (A.2)), we obtain

$$\begin{aligned} S_E &= \int_{[0,\beta]\times V} d^4x_E \left(\frac{1}{\sqrt{V}}\sum_{\vec{p}',m} e^{i\left(\omega_m\tau-\vec{p}'\vec{x}\right)}\overline{\psi}_m(\vec{p}')\right) S^{-1}\left(\frac{1}{\sqrt{V}}\sum_{\vec{p},n} e^{-i(\omega_n\tau-\vec{p}\vec{x})}\psi_n(\vec{p})\right) \\ &= \int_{[0,\beta]\times V} d^4x_E \left(\frac{1}{\sqrt{V}}\sum_{\vec{p}',m} e^{i\left(\omega_m\tau-\vec{p}'\vec{x}\right)}\overline{\psi}_m(\vec{p}')\right)\left(-\gamma^0\partial_\tau+\gamma^0\mu+i\gamma^j\partial_j-\sum_{\vec{q}} e^{i\vec{q}\vec{x}}M_{\vec{q}}\right)\left(\frac{1}{\sqrt{V}}\sum_{\vec{p},n} e^{-i(\omega_n\tau-\vec{p}\vec{x})}\psi_n(\vec{p})\right) \\ &= \frac{1}{V}\int_{[0,\beta]\times V} d^4x_E \sum_{\vec{p},\vec{p}',m,n} e^{i\left((\omega_m-\omega_n)\tau+\left(\vec{p}-\vec{p}'\right)\vec{x}\right)}\overline{\psi}_m(\vec{p}')\left(i\gamma^0\omega_n+\gamma^0\mu-\gamma^j p_j-\sum_{\vec{q}} e^{i\vec{q}\vec{x}}M_{\vec{q}}\right)\psi_n(\vec{p})\,, \end{aligned} \tag{B.1}$$

Now, we are able to perform the integration over the imaginary time trivially as we identify the integral representation of the Kronecker-Delta with respect to the Matsubara frequencies. Yet, we have to be careful regarding the integration over position space. To address that, we separate the mass function from the other three summands and integrate them separately

$$S_{E,1} = \int_V d^3x\, e^{i\left(\vec{p}-\vec{p}'\right)\vec{x}}\overline{\psi}_n(\vec{p}')\left(i\gamma^0\omega_n-\gamma^j p_j+\gamma^0\mu\right)\psi_n(\vec{p}) = V\overline{\psi}_n(\vec{p}')\left(i\gamma^0\omega_n-\gamma^j p_j+\gamma^0\mu\right)\delta_{\vec{p},\vec{p}'}\psi_n(\vec{p}) \tag{B.2}$$

$$S_{E,2} = -\int_V d^3x\,\overline{\psi}_n(\vec{p}')\left(\sum_{\vec{q}} e^{i\left(\vec{p}+\vec{q}-\vec{p}'\right)\vec{x}}M_{\vec{q}}\right)\psi_n(\vec{p}) = -V\,\overline{\psi}_n(\vec{p}')\left(\sum_{\vec{q}} M_{\vec{q}}\delta_{\vec{p},\vec{p}'-\vec{q}}\right)\psi_n(\vec{p})\,. \tag{B.3}$$

This leads to

$$S_E = \frac{\beta}{V}\sum_{\vec{p},\vec{p}',n}\left(S_{E,1}+S_{E,2}\right) = \beta\sum_{\vec{p},\vec{p}',n}\overline{\psi}_n(\vec{p}')\left(\left(i\gamma^0\omega_n-\gamma^j p_j+\gamma^0\mu\right)\delta_{\vec{p},\vec{p}'}-\left(\sum_{\vec{q}} M_{\vec{q}}\delta_{\vec{p},\vec{p}'-\vec{q}}\right)\right)\psi_n(\vec{p}) \tag{B.4}$$

$$= \beta\sum_{\vec{p},\vec{p}',n}\overline{\psi}_n(\vec{p}')S^{-1}_{p,p',n}\psi_n(\vec{p})\,, \tag{B.5}$$

where $S^{-1}_{p,p',n}$ denotes the inverse quark propagator in frequency-momentum space. Plugging this result into our partition function (eq. (2.12)) and performing the functional integral yields

$$\mathcal{Z} = \int \mathcal{D}\overline{\psi}_n(\vec{p}')\,\mathcal{D}\psi_n(\vec{p})\,\exp\left(\beta\sum_{\vec{p},\vec{p}',n}\overline{\psi}_n(\vec{p}')S^{-1}_{p,p',n}\psi_n(\vec{p})\right) = \det\beta S^{-1}_{p,p',n}\,. \tag{B.6}$$

B.2 Calculating the Sum Over the Matsubara Frequencies

After having calculated the trace over frequency-momentum and Dirac space in the previous section, our final step is to calculate the sum over the fermionic Matsubara frequencies

$$\sum_n \log\left(\beta^4\left(\omega_n - i\,\mu + i\,E_\nu\right)\right). \tag{B.7}$$

To calculate it, we start with differentiating the sum with respect to E_λ

$$\frac{\partial}{\partial E_\lambda}\sum_n \log\left(\beta^4\left(\omega_n - i\,\mu + i\,E_\nu\right)\right) = \sum_n \frac{i}{\omega_n - i\,\mu + i\,E_\nu} = \sum_n \frac{1}{E_\nu - (i\,\omega_n + \mu)}\,. \tag{B.8}$$

Now we will use the residue theorem "backwards", i.e. find a function $f(z)$ to which eq. (B.8) are the residues. One possibility is [32]

$$f(z) = \frac{\beta}{2}\tanh\left(\beta\,\frac{z-\mu}{2}\right)\cdot\frac{1}{E_\nu - z}\,, \tag{B.9}$$

if the contour $\mathscr{C}_1$ is chosen in a such way that it contains the poles $z_n = i\omega_n + \mu$, but not the pole $z_\lambda = E_\nu$. From the residue theorem it follows that

$$\frac{1}{2\pi i}\oint_{\mathscr{C}_1} dz\, f(z) = \sum_a \mathrm{res}_a\, f = \sum_n \mathrm{res}_{i\omega_n+\mu} f = \sum_n \frac{1}{E_\nu - (i\,\omega_n + \mu)}$$

holds. We are now able to transform the contour $\mathscr{C}_1$ into a new contour $\mathscr{C}_2$ which does not contain the points $z_n = i\omega_n + \mu$, but which does encircle the pole z_λ clockwise. The resulting residue yields

$$\mathrm{res}_{E_\nu} f = \lim_{z\to E_\nu}(z - E_\nu)\, f(z) = \frac{\beta}{2}\tanh\left(\beta\,\frac{E_\nu - \mu}{2}\right). \tag{B.10}$$

Therefore we can rewrite our sum over the Matsubara frequencies as

$$\frac{1}{2\pi i}\oint_{\mathscr{C}_1} dz\, f(z) = \sum_n \frac{1}{E_\nu - (i\,\omega_n + \mu)} = \frac{1}{2\pi i}\oint_{\mathscr{C}_2} dz\, f(z) = \frac{\beta}{2}\tanh\left(\beta\,\frac{E_\nu - \mu}{2}\right). \tag{B.11}$$

Our final task is to integrate the newly found residues with respect to E_ν in order to reobtain our original expression, which is readily done

$$\sum_n \log\left(\beta^4\left(\omega_n - i\,\mu + i\,E_\nu\right)\right) = \log\left[2\,\cosh\left(\beta\,\frac{E_\nu - \mu}{2}\right)\right]. \tag{B.12}$$

Hence, we have finally calculated a general expression for the kinetic part of the grand potential (eq. (2.14)):

$$\Omega_{kin} = -\frac{N_c N_f}{\beta V}\sum_{E_\nu} \log\left[2\,\cosh\left(\beta\,\frac{E_\nu - \mu}{2}\right)\right]. \tag{B.13}$$

C Parameters

C.1 Parameter Sets

In the course of this work we use parameters that are fitted for the chiral limit to reproduce a constituent quark mass of 300 MeV at a temperature and chemical potential of 0. However, we also briefly use parameter sets for an enforced constituent quark mass of 330 and 250 MeV, respectively, for comparison. Moreover all parameter sets were fitted to enforce a pion decay constant in the vacuum and the chiral limit of $f_\pi = 88$ MeV.

#	M_{vac} /MeV	Λ /MeV	$G_S \Lambda^2$
1	300	757.048	6.002
2	250	856.706	5.09871
3	330	728.4	6.6

Table C.1.: Parameter sets used in this work.

C.2 Pauli-Villars-Coefficients

Throughout this work we make use of the Pauli-Villars (PV) regularization scheme.
In general, the PV-coefficients are calculated by expanding the replacement term for large energies E, i.e. around $x = \frac{\Lambda^2}{E^2} = 0$, where Λ denotes the Pauli-Villars cutoff parameter, up to the order $(n-1)$ in x

$$f_{PV}(E) = \sum_{j=0}^{n} c_j \sqrt{E^2 + j\Lambda^2} = E \sum_{j=0}^{n} c_j \sqrt{1 + jx} = E \sum_{j=0}^{n} c_j \left(1 + a_1\, j\, x + a_2\, j^2\, x^2 + ... + a_{n-1}\, j^{n-1}\, x^{n-1} + \mathcal{O}(x^n)\right) , \quad \text{(C.1)}$$

where n denotes the number of PV-coefficients and a_i, $i \in \{1, 2, ..., n-1\}$ are constant factors resulting from the expansion. Fixing the zeroth coefficient c_0 to an arbitrary, finite value, we are able to determine the PV-coefficients by equating the resulting n expansion coefficients to zero. Since constant factors do not affect the roots of an equation, we can omit the factors a_i. Therefore, in general, one has to solve the equations

$$\sum_{j=0}^{n} c_j = \sum_{j=0}^{n} c_j j = \sum_{j=0}^{n} c_j j^2 = \sum_{j=0}^{n} c_j j^3 = ... = \sum_{j=0}^{n} c_j j^{n-1} = 0$$

self-consistently in order to obtain the n PV-coefficients. It is noteworthy that those equations only determine the PV-coefficients up to a constant factor which equals the zeroth coefficient c_0.
In this work we use three PV-coefficients and thus have to solve

$$\sum_{j=0}^{3} c_j = \sum_{j=0}^{3} c_j j = \sum_{j=0}^{3} c_j j^2 = 0 ,$$

self-consistently. Fixing the zeroth coefficient to be $c_0 = 1$, which reflects our original term, we obtain $c_1 = -3$, $c_2 = 3$ and $c_3 = -1$.

Bibliography

[1] J. Thomson, *Phil.Mag.* **44**, 293–316 (1897).

[2] E. Rutherford, *Phil.Mag.* **21**, 669–688 (1911).

[3] E. Rutherford, *Philosophical Magazine Series 6* **37**, 581–587 (1919).

[4] J. Chadwick, *Nature* **129**, 312 (1932).

[5] W. Heisenberg, *Zeitschrift für Physik* **77**, 1–11 (1932).

[6] M. Gell-Mann, *Phys.Lett.* **8**, 214–215 (1964).

[7] G. Zweig, *CERN-TH-401* (1964).

[8] G. Zweig, *Developments in the Quark Theory of Hadrons* **1**, 22–101 (1964).

[9] M. Breidenbach, J. I. Friedman, H. W. Kendall, E. D. Bloom, D. H. Coward, H. DeStaebler, J. Drees, L. W. Mo and R. E. Taylor, *Phys. Rev. Lett.* **23**, 935–939 (1969).

[10] E. D. Bloom, D. H. Coward, H. DeStaebler, J. Drees, G. Miller, L. W. Mo, R. E. Taylor, M. Breidenbach, J. I. Friedman, G. C. Hartmann and H. W. Kendall, *Phys. Rev. Lett.* **23**, 930–934 (1969).

[11] H. Fritzsch, M. Gell-Mann and H. Leutwyler, *Phys.Lett.* **B47**, 365–368 (1973).

[12] P. Braun-Munzinger and J. Wambach, *Rev.Mod.Phys.* **81**, 1031–1050 (2009), arXiv:0801.4256.

[13] F. Karsch, *Lect.Notes Phys.* **583**, 209–249 (2002), arXiv:hep-lat/0106019.

[14] U. Vogl and W. Weise, *Prog.Part.Nucl.Phys.* **27**, 195–272 (1991).

[15] S. Carignano and M. Buballa, *Acta Phys. Pol. B Proc. Suppl.* **5**, 641 (2011), arXiv:1111.4400.

[16] Y. Nambu and G. Jona-Lasinio, *Phys. Rev.* **122**, 345–358 (1961).

[17] Y. Nambu and G. Jona-Lasinio, *Phys. Rev.* **124**, 246–254 (1961).

[18] S. Klimt, M. Lutz, U. Vogl and W. Weise, *Nuclear Physics A* **516**, 429–468 (1990).

[19] U. Vogl, M. Lutz, S. Klimt and W. Weise, *Nuclear Physics A* **516**, 469–495 (1990).

[20] J. Goldstone, A. Salam and S. Weinberg, *Phys. Rev.* **127**, 965–970 (1962).

[21] M. Buballa and S. Carignano, *Prog.Part.Nucl.Phys.* **81**, 39–96 (2015), arXiv:1406.1367.

[22] J. I. Kapusta and C. Gale, *Finite-Temperature Field Theory: Principles and Applications (Cambridge Monographs on Mathematical Physics)*, Cambridge University Press (2006).

[23] S. Klevansky, *Rev. Mod. Phys.* **64**, 649–708 (1992).

[24] D. Nickel, *Phys.Rev.D* **80** (2009), arXiv:0906.5295.

[25] M. Kutschera, W. Broniowski and A. Kotlorz, *Nuclear Physics A* **516**, 566 – 588 (1990).

[26] S. Carignano, *Inhomogeneous Chiral Symmetry Breaking Phases*, PhD thesis, TU Darmstadt (2012).

[27] D. Nickel and M. Buballa, *Phys.Rev.D* **79** (2008), arXiv:0811.2400.

[28] S. Carignano and M. Buballa, *Phys.Rev.* **D86**, 074018 (2012), arXiv:1203.5343.

[29] E. Nakano and T. Tatsumi, *Phys.Rev.D* **71** (Phys.Rev.D71:114006,2005), arXiv:hep-ph/0411350.

[30] T. Kojo, Y. Hidaka, L. McLerran and R. D. Pisarski, *Nucl.Phys.* **A843**, 37–58 (2010), arXiv:0912.3800.

[31] M. Sadzikowski and W. Broniowski, *Phys.Lett.* **B488**, 63–67 (2000), arXiv:hep-ph/0003282.

[32] A. Altland and B. D. Simons, *Condensed Matter Field Theory*, Cambridge University Press (2010).